Analysis and Design of Substrate Integrated Waveguide-based Antennas for Millimeter Wave Applications

Shraman Gupta

A Thesis

in

The Department

Of

Electrical and Computer Engineering

Presented in Partial Fulfillment of the requirements

For the degree of Master in Applied Science (Electrical Engineering) at

Concordia University

Montreal, Quebec, Canada

May 2016

CONCORDIA UNIVERSITY
SCHOOL OF GRADUATE STUDIES

This is to certify that the thesis prepared

By: Shraman Gupta

Entitled: "Analysis and Design of Substrate Integrated Waveguide-based Antennas For Millimeter Wave Applications"

and submitted in partial fulfillment of the requirements for the degree of

Master of Applied Science

Complies with the regulations of this University and meets the accepted standards with respect to originality and quality.

Signed by the final examining committee:

_____ Chair
Dr. R. Raut

_____ Examiner, External
Dr. A. K. Waizuddin (MIE) To the Program

_____ Examiner
Dr. R. Paknys

_____ Supervisor
Dr. A. Sebak

Approved by: _____
Dr. W. E. Lynch, Chair
Department of Electrical and Computer Engineering

_____20_____ _____
Dr. Amir Asif, Dean
Faculty of Engineering and Computer Science

Abstract

Analysis and Design of Substrate Integrated Waveguide-based Antennas for Millimeter Wave Applications

Shraman Gupta

Concordia University.

Recently, there has been increasing interest and rapid growth in millimeter wave (MMW) antennas and devices for use in diverse applications, services and technologies such as short-range communication, future mm-wave mobile communication for the fifth generation (5G) cellular networks, and sensor and imaging systems. Due to the corresponding smaller wavelength, mm-wave frequencies offer the advantage of physically smaller antennas and circuits as well as the availability of much wider bandwidth compared to microwave frequencies. It is important to design millimeter wave antennas with high gain characteristics due to their high sensitivity towards atmospheric absorption losses. Moreover, millimeter wave antennas can have wide bandwidth and are suitable for applications in large frequency range.

In this thesis, planar antennas are designed using substrate integrated waveguide (SIW) technology to have low losses, high quality factor, and low fabrication cost. Firstly, an antipodal fermi linear tapered slot antenna (AFLSTA) with sine corrugations at the side edges at 32.5 GHz is presented, which has a wide impedance bandwidth greater than 30 %, in order to support the high data rate channels. This antenna has a high gain of 12.6 dB and low side lobe levels (better than - 17 dB) in both E and H planes. This antenna is studied and analyzed in array and beamforming configurations to meet requirements of millimeter wave applications.

In order to obtain high gain and narrow beamwidth pattern, a 1 × 8 AFLTSA array using SIW power divider network is presented. The design characteristics of the power divider network are presented in this thesis, which help in calculating the performance characteristics of this array structure. This array has an acceptable bandwidth of 14.7 % (30-35 GHz) with high gain of 20.4 dB and 8.35° 3 dB beamwidth. The side lobe levels are also improved using this SIW power divider network and are lower than -25 dB in E-plane and -15 dB in H-plane respectively. This antenna has a radiation efficiency greater than 93% over the whole bandwidth.

The second research theme is beamforming of AFLTSA antenna. This beamforming is performed using multi-beam antenna concept in which the beam is rotated with a help of compact beamforming network and excitation from different input ports. The design methodology for 2 × 2 and 4 × 4 subarray beamforming networks is presented along with their current distributions illustrating the beamforming process. These subarrays possess wide impedance bandwidth between 29-36 GHz. Moreover, these subarrays are able to achieve gain between 12-15 dB with narrow beamwidth reaching till 11°. All the results along with the numerical data is presented in this thesis. This antenna is suitable candidate for millimeter wave wireless communications and imaging systems.

Acknowledgement

Firstly, I would like to express my deepest gratitude and thanks to my supervisor Dr. A.R Sebak for his continuous and generous support throughout my student life at Concordia University. I am grateful to him for allowing me to work on technologies related to millimeter wave antennas whose fabrication and measurement process is complex. His supporting nature and knowledge helped me to learn and analyze this area of specialization.

Besides my supervisor, I would like to thank Dr. Ahmed Kishk for enhancing my microwave skills during my Master of Engineering period. I would like to express my deepest appreciation to my colleagues in the electromagnetic group specially, Mohammad Akbari Choubar and Zouhair Briqech for their motivation and sharing their knowledge and experience to complete my work within time.

Also, I would like to thank Mr. Jeff Landry and Mr. Dave Chu for helping me in fabrication process along with my special gratitude to Mr. Vincent Mooney-Chopin for helping me to understand measurement procedures.

Finally, I would like to thanks my parents, my wife and almighty for encouragement and support without whom this wouldn't have been possible.

Table of Contents

List of Figures

List of Tables

List of Abbreviations

AFLTSA	Antipodal Fermi Linear Tapered Slot Antenna
AFTSA	Antipodal Fermi Tapered Slot Antenna
ALTSA	Antipodal Linear Tapered Slot Antenna
BFN	Beamforming Networks
CAD	Computer Aided Design
CMOS	Complementary metal–oxide–semiconductor
CPW	Coplanar waveguide
CST	Computer Simulation Techniques
DRA	Dielectric Resonator Antenna
DVLTSA	Dual V-type linear TSA
EHF	Extremely High Frequency
FCC	Federal Communications Commission
FDTD	Finite Difference Time Domain
FEM	Finite Element Method
FIT	Finite Integration Technique
FM	Frequency Modulation
GCPW	Grounded Coplanar Waveguide
HFSS	High Frequency Electromagnetic Field Simulation
IMT	International Mobile Telecommunications
ITS	Intelligent Transport Systems
LAN	Local Access Network

LMDS	local multipoint distribution system
LTE	Long-Term Evolution
MIMO	Multiple Input Multiple Output
MMW	Millimeter wave
MoM	Method of Moment
PCS	Printed Circuit Board
SIC	Substrate Integrated Circuits
SIW	Substrate Integrated Waveguide
SLL	Side Lobe Level
TSA	Tapered Slot Antenna
UHF	Ultra-High Frequency

Chapter1: Introduction

1.1 Introduction

Wireless communications have been rapidly increasing and developing since 1980 with the first development of 1G network. Wireless communications has reached a level of 4G network till date, which has been designed to meet the requirements of wireless standards such as IEEE 802.16m and LTE-Advanced requirements [1]. Nowadays, mobile phones and wireless networks can be found everywhere. The fast and quick communication have been in tremendous demand for wireless networks. For this reason, the main challenges for the future wireless system developers are the growing need for higher transmission rates and the increasing number of users. For example, there is a requirement of very high data transmission (more than 1Gbps) for wireless transmission of the uncompressed high-definition video image. It is difficult to achieve such transmission data rate because of the conventional wireless systems using frequencies up to 10 GHz due to limited bandwidth [2]. One of the possible solutions to achieve this high data transmission problem is the use of millimeter wave frequency technology (30 GHz – 300 GHz) that can provide large bandwidths, single chip integration due to small guided wavelength λ of 1-10 mm. This small guided wavelength limits the millimeter wave communication systems especially the short range communications due to high loss in free space i.e. wall penetration loss whereas it is beneficial for outdoor point to point links when high directive antennas can be utilized [3].

The wireless communication has been evolved, as shown in Fig 1.1 since 1980 through its analog technology with an introduction of 1G network, which was designed for voice communications only., 2G systems were introduced through the use of digital modulations and time division or code division multiple access (CDMA) to provide data services and improved spectral efficiency.

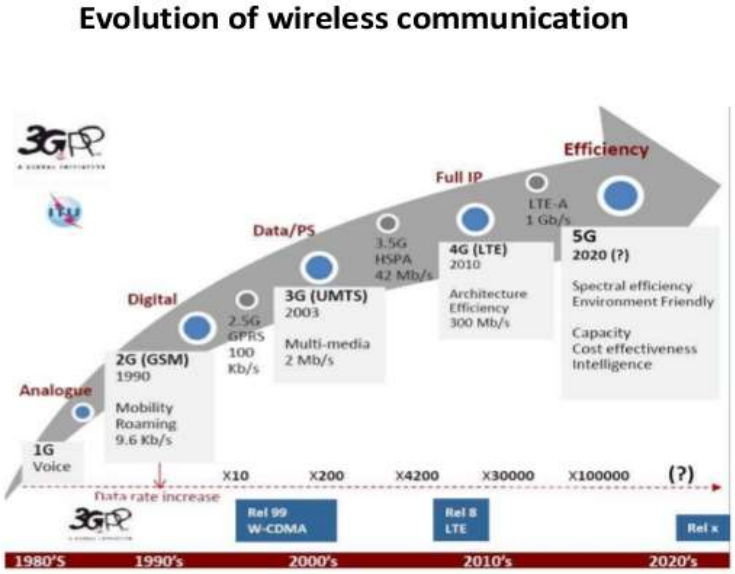

Fig 1.1 Evolution of wireless communication [3]

In early 2000's, 3G network system was introduced, which could provide high speed data transmission for both videos and audio streaming capabilities using technologies such as W-CDMA and HSPA, which was later evolved in 2008 for improving the performance of 3G mobile telecommunications. The next generation, used for implementing so called 4G network, is IMT-Advanced (International Mobile Telecommunications-Advanced) technology along with the LTE radio access technology. LTE is an orthogonal frequency division multiplexing based radio access technology that supports bandwidth up to 20 MHz. The major inclusion of multiple input multiple output (MIMO) enables 4G systems

to work with high data rates with high spectral efficiency, improved link quality and adapted radiation patterns for signal gain and interference [4].

There are three stages for wireless communications to execute: transmission, propagation and reception. A low frequency signal is transmitted through the antenna and the transmitter modulates this signal with the high frequency carrier signal and sends out in the space, where the signal is propagated in the form of waves. At this stage, the signal can be perturbed from atmospheric conditions and results in high losses as there is an increase in the frequency. The signal is demodulated and received at the receiver side and the whole wireless communication process is carried out in a similar way [1].

1.2 Brief overview of millimeter wave communications

Many current wireless systems operate at high frequency (3MHz to 30MHz), very high frequency (30MHz to 300MHz) and ultra-high frequency (300MHz to 3GHz) bands [2]. However, there is a need to go beyond such frequency spectrum to meet today's need. Therefore, to meet the bandwidth requirements, the service providers face a huge challenge to overcome these rapid changes in mobile data growth. Besides, all wireless devices are limited to a carrier frequency spectrum ranging between 700 MHz and 2.6 GHz.

Recent studies suggest that millimeter wave frequencies could be used as a possible solution to future wireless networks congestion that only work in a frequency spectrum of 30 GHz – 300 GHz [1]. It is not only the millimeter wave frequency range but also highly directional beamforming antennas, lower outage probability, higher bit rates covering larger areas and lower infrastructure costs, which will contribute to the advancement of new 5G network [1]. In combination with the CMOS technology, which can operate efficiently in millimeter wave frequency bands, the steerable antennas strengthens the

feasibility of millimeter wave wireless communications [5]. This frequency range helps to expand channel bandwidths, which increases the data capacity for solving the data congestion issue. It is possible to exploit techniques such as polarization and new spatial techniques like massive MIMO (multiple inputs multiple outputs) and adaptive beamforming [6] at this frequency spectrum.

Millimeter wave antennas are designed at millimeter wave frequency spectrum, also known as extremely high frequency (EHF) band, which have high gain to counter the propagation losses issue in the free space. A low cost millimeter wave antenna is desired, which should be planar and easy to fabricate to have a low profile and low insertion losses. Currently, most of the research work is based on 28 GHz band, 38 GHz band, 60 GHz band and E-band (71-76 GHz and 81-86 GHz). The standards such as ECMA -87 [7], IEEE 802.15.3c [8] and IEEE 802.11ad [9] are considered to meet the frequency spectrum requirements at millimeter wave band especially for EPAN and WLAN.. Most of the work is focused on 28 GHz and 38 GHz band because of the following reasons:

a) Millimeter wave communications is very promising for the local multipoint distribution system (LMDS) concept, which operates between 20 to 40 GHz [10] and moreover, this area is unused or underutilized in mobile communications [11].
b) There are regional regulatory status and availability of licensed spectrum for 28 GHz and 38 GHz with an availability of standardized components at this frequency range [1].
c) There is low atmospheric absorption as compared to 60 GHz frequency spectrum and comparable free space path loss as of today's 1-2 GHz spectrum [12].

d) Rain attenuation and oxygen loss do not significantly increase at 28 GHz, and there will be better propagation conditions as compared to today's cellular networks when one considers the availability of high gain adaptive antennas and cell sizes of the order of 200 meters [11] [12].

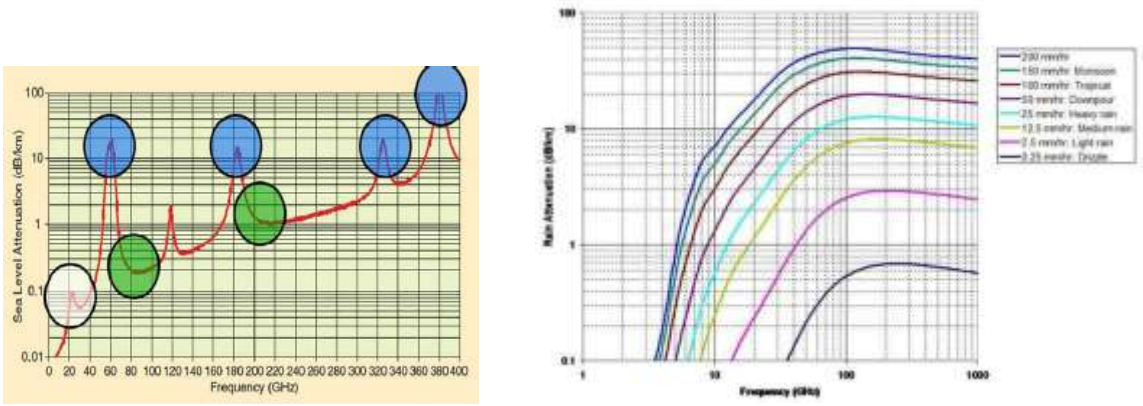

Fig. 1.2 Atmospheric attenuation curve (left) and rain attenuation curve (right) for millimeter waves [1]

1.3 Motivation

1.3.1 Need for millimeter wave communications

The need in applications such as satellite communications and mobile telecommunications has recently increased the attention of network industries to come up with solutions that can utilize an underutilized spectrum in the millimeter wave frequency band. This frequency band can be referred to as extremely high frequency (EHF) band with large frequency spectrum from 30 GHz to 300 GHz [3]. The high frequency of millimeter waves as well as their propagation characteristics (i.e. the ways they change or interact with the atmosphere as they travel) makes them useful for a variety of applications including transmitting large amounts of computer data, cellular communications, and radar applications.

The advantages and disadvantages of millimeter wave frequency to achieve high data transmission rates are listed as follows:

The advantages of millimeter wave communications are:

1. The guided wavelength is small for this frequency spectrum, which results in the small size of antennas i.e. compactness is achieved concerning the antenna size and integrated parts packaging.
2. Larger bandwidths can be obtained at millimeter wave frequency spectrum [13].
3. It is beneficial for short distance data exchanges which can be obtained with extreme data rates [14].
4. Narrow beamwidth can be obtained at this frequency spectrum which can be well suited for networks topologies such as point to point mesh, a dense hub, and spoke or even a ring.
5. There are inherently directional and electronically steerable antenna arrays that are realized as patterns on printed circuit board.

The disadvantages are:

1. At high frequencies, the signals are sensitive to blockages by obstacles due to weak diffraction ability [1].
2. Due to smaller wavelength and compact antenna, a greater precision of manufacturing and prototyping is required which increases the developing cost of the antenna.
3. It suffers from huge propagation loss and can be limited by atmospheric attenuation without using adapting beamforming technique, which makes it directional [1,13].

4. Loss factor in free space is directly proportional to the square of operating frequency as per Friis transmission equation.
5. Narrow beamwidth can lead to a problem in target search and acquisition. Thus, millimeter waves are not suitable for large volume search [15].

1.3.2 Millimeter Wave Technology Applications

Due to increased demand for higher data rates and to operate at higher frequency spectrum (mm-wave spectrum), it has been used in different types of applications. Some of them are listed below:

1. **Communications:** It is used in wireless communication systems especially terrestrial and satellite communications, and wireless data transmission. The data rates may reach 40 to 100 times higher than that of wireless LAN [1].
2. **Sensors:** Millimeter wave technology can be used in Intelligent Transport Systems (ITS) due to its ability to function well in adverse weather conditions. This technique includes applications like automotive radar and infrastructure radar systems. It also includes applications such as autonomous cruise control, speed and range sensors for industrial usages, aircraft anti-collision sensor, robotic vision, imaging, motion sensors, safety and security sensors and much more [3].
3. **Studies and Experiments:** This technology is used to have more precise results in magnetic resonance operating at very high frequency range, which helps to obtain a better resolution spectral and sensitivity towards experiments [15].
4. **Weapon systems:** One of the primary application of this millimeter wave technology is Active Denial System (ADS), U.S. Air Force weapons systems having 3 mm wavelength. Other applications are missile guidance, navigation

guidance, surveillance systems for air defense, and location tracking for snipers [12].

The applications of millimeter wave technology has been proposed for 5G wireless network communications as explained below:

1. To meet the demands of data usage, a ten thousand fold increase in capacity has been proposed by 2030 with massive densification of small cells [2]. In this literature, the focus is given on millimeter wave technology at 5G enhanced local area (eLA) access, which could achieve peak data rates over 10 Gbps and edge data rates of more than 100 Mbps. Millimeter wave technology can support multi gigabit rates and high multimedia applications because of its large bandwidth.
2. Another research was conducted on uncompressed high-definition (HD) video up to 3 Gb/s [16].
3. The broad bandwidth is very useful for this technology to provide possible support to 5G cellular access and as explained in [1], to provide a high radiation efficiency to suppress the atmospheric absorption losses.
4. The gain based on arbitrary pointing angles of directional antennas is 20 times greater than 4G LTE networks and can be further improved if they point in the direction of maximum radiation [11].
5. It is very advantageous to use a device to device (D2D) communications for millimeter wave technology, as it saves power in close proximity and also improves spectral efficiency [3].
6. It is very costly to connect 5G base stations to another 5Gs base stations and the network by fiber based backhaul [17]. Therefore, more cost effective and flexible

high speed wireless backhaul is used, which provides higher Giga bit rates and can be a possible solution to backhaul of small cells.

1.4 Thesis Objectives

The primary goal of the work presented in this thesis is the design and implementation of end-fire radiation based antennas for millimeter wave frequency band (basically at 30 GHz i.e. Ka-band) with focus on the following two tasks:

a) The antenna should have high gain to meet high atmospheric absorption and attenuation losses at millimeter wave frequencies. Besides high gain antenna, it is important to achieve wide bandwidth performance with lower side lobe levels to support high data rates. In a view to achieve high gain, millimeter wave based array systems are designed. These array systems should have low side lobe level and narrow beamwidth, and it can be attained using substrate integrated technology. The objective is to achieve gain around ~20 dB and side lobe level better than -20 dB in both E- and H-planes.

b) The other aspect of research deals with beamforming structures for endfire radiation based antennas. The objective is to achieve high gain and narrow beamwidth for subarray beamforming networks at millimeter wave (MMW). It can be realized by designing the SIW based multimode section using s-parameters technique and this work is fabricated and measured for both the 2 × 2 and 4 × 4 subarray structures.

The antenna used for achieving the above said objectives is Antipodal Fermi Linear Tapered Slot Antenna (AFLTSA) at a frequency of 32.5 GHz. Therefore, a different type of array structures is designed and implemented to achieve high gain, wide impedance

bandwidth, and narrow beamwidth along with beamforming operation for millimeter wave technology.

1.5 Thesis Organization

This thesis is mainly divided into six chapters as follows:

Chapter 2 provides a literature review on millimeter wave technology based antennas. This chapter introduces different types of antennas that can be used at millimeter wave frequency band and explain the difference between endfire and broadside radiation based antennas. This chapter further gives insight on millimeter wave based array systems and beamforming networks to achieve above stated thesis objectives.

Chapter 3 presents research methodology or theoretical knowledge needed to achieve the above-stated objectives. This chapter includes basic antenna theory along with numerical techniques used for full wave analysis including Maxwell equations. Furthermore, the design methodology for substrate integrated waveguide (SIW) based antennas and their array systems and beamforming techniques is explained in this chapter. Besides, the design of single element antenna, AFLTSA, is also presented in this chapter along with the simulated results using Ansys HFSS and CST Microwave Studio simulation software.

Chapter 4 presents with the 1 × 8 AFLTSA array structure based on substrate integrated technology using Dolph-Chebyshev techniques. This chapter provide the design of SIW power divider along with the proposed antenna array and its parametric study analysis. Later the results are presented using both the simulation software which shows the practical aspect of this proposed work.

Chapter 5 presents the 2 × 2 and 4 × 4 subarray structures based on substrate integrated waveguide technology for beamforming operation. The design methodology is presented together with the parametric analysis for both the subarray structures. Later the fabrication and measurement setup requirements for this type of antenna structures are discussed. Finally, the measured and simulated results are compared with this proposed work.

Chapter 6 presents the thesis' conclusion and also presents the contributions and future works for this proposed work to achieve more practical and advanced antennas for 5G telecommunications, and detection and precise target tracking based applications.

Chapter 2: Literature Review

2.1 Millimeter wave wireless communications

There has been an evolution of millimeter wave (MMW) wireless networks in modern communications. Guglielmo Marconi developed the first wireless telegraph communication systems in the early 1900sthat depicted the expansion from point to point technologies to radio broadcast systems and finally to wireless systems. In today's world, one can find himself in a world of wireless networking, mostly with the use of cellular networks, WLAN and personal area networks that were developed in last twenty years. The advancement in technology has caused the device makers, infrastructure developers and manufacturers to look for the solutions that can have greater bandwidth allocation spectrum to achieve the data demands with respect to the data capacity available in today's licensed spectrum [3].

Historically, the millimeter wave frequencies were used mostly for defense and radio astronomy applications mainly because of high cost and limited availability of electronic devices. Although currently, due to advances in silicon technology and an urgent need for mm-wave frequency spectrum, it can be used for applications such as automotive radars, high-resolution imaging and high definition video transfer for which highly integrated, low power and low-cost wireless systems are required that include high gain and efficient planar antennas. The small wavelength at mm-wave frequencies results in small and compact antennas. The size of an antenna is determined by the order of wavelength, for instance for mm-wave frequency spectrum (30-300 GHz), the wavelength varies between 10-1 mm. It is easy to design antennas of this size and radiate efficiently with wide

impedance bandwidth and narrow beamwidth. However, the radiation losses increase with an increase in frequency; therefore, an antenna designer has to be careful while designing the antennas at this frequency spectrum. Therefore, it is critical to choose the type of antenna for mm-wave frequency range, which possesses high gain and wide bandwidth as there will be an increase in gain and radiation losses but decrease in bandwidth for an array based antenna system. Therefore, firstly, a literature study, explained in this chapter, is done on different types of antennas such as horn antenna, lens antenna, aperture coupled antenna, dielectric resonator antennas (DRA), microstrip based antennas, substrate integrated waveguide (SIW) antenna and tapered slot antenna (TSA), etc. Later, a study is done on millimeter wave based array antenna structures to achieve the desired objective of high gain. But there are chances of reducing the bandwidth; therefore, an acceptable bandwidth allocation should be desired that can be effectively done by designing antennas with low side lobe levels (better than 20-30 dB). The desired low side lobe level can be achieved by designing power divider using Dolph-Chebyshev, Taylor distributions, binomial distributions etc. Finally, a literature study is conducted on millimeter wave based beamforming networks, which includes subarray structures to keep high gain but also able to perform beam rotation for applications such as image detection or precise target tracking.

2.2 MMW technology based antennas

In this section, a brief overview of millimeter wave antenna is presented. In general for non-scanning applications, there are two types of antennas, based on their radiation patterns, which can be classified as broadside and endfire antennas.

2.2.1 Microstrip antennas

This type of antenna is one of the most widely used type of antenna that fulfills most of the current wireless systems requirements. These antennas are also called patch antennas [18] and are widely used in wireless communication systems such as mobile and satellite communications. By definition, microstrip antennas consist of a thin sheet of low loss insulating material called dielectric substrate and completely covered with a metal on one side called the ground plane and partially metalized on the other side as per the design of the feeding network [19].

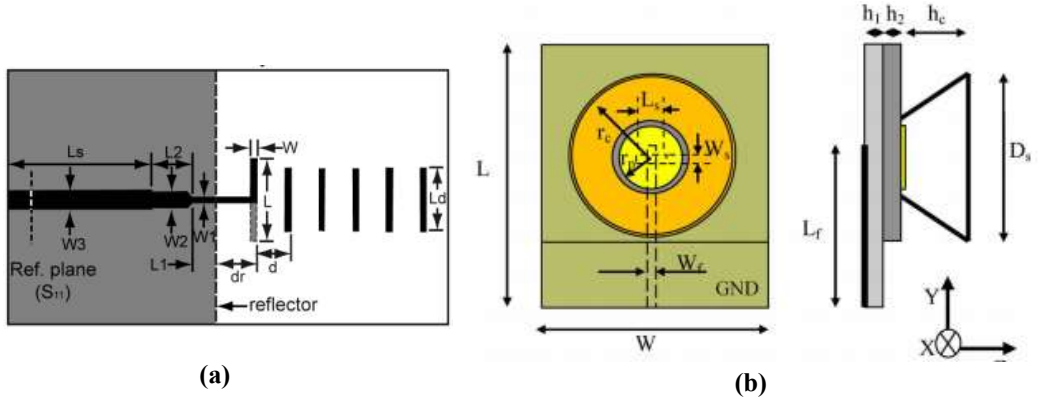

Fig. 2.1 (a) Yagi-Uda antenna for switched beam systems [20] (b) Hybrid Microstrip/Conical patch antenna [21]

For instance, Yagi-Uda antenna for millimeter wave switched beam systems [20], which is suitable for mm-wave radars and high data rate communication systems as shown in Fig 2.1 (a).This configuration has endfire radiation and possesses a measured gain of 9-10 dB and 17 % bandwidth for a single element and a measured gain of 11.5-13 dB for two element array at proposed 24 GHz. In one of the works for broadside radiation in [21], a circular patch antenna at 31 GHz with a gain of 6 dB is presented and in order to enhance the gain by 6 dB more, a conical horn is placed over the conventional circular patch

antenna. These two designs present the narrow bandwidth using microstrip based antenna of around 1-2 GHz; therefore, an integration of other antennas such as TSA, AFTSA or AFLTSA is implemented to increase the bandwidth as well as the gain of single element antenna.

2.2.2 Dielectric Resonator Antennas (DRA)

Such antennas are generally used for broadside type of radiation for all frequency ranges. DRAs have a tendency to radiate efficiently at high frequency [22], making them attractive for millimeter wave applications such as wireless communications, microwave imaging, and hidden objects detection. This category of antenna has fewer conductor losses and larger bandwidth as compared to microstrip patch antennas [23] but has a lower profile than reflector and horn antennas. In this paper [23], as shown in Fig 2.2, the measured bandwidth (S_{11} < -10 dB) is 2.6 % and 15.6 % but the gain achieved is 7.1 dB and 6.9 dB for a circular patch and cylindrical DRA respectively at 35.5 GHz. But the cylindrical DRA has higher radiation efficiency (94.9%) as compared to circular disk patch antenna (78.2%).

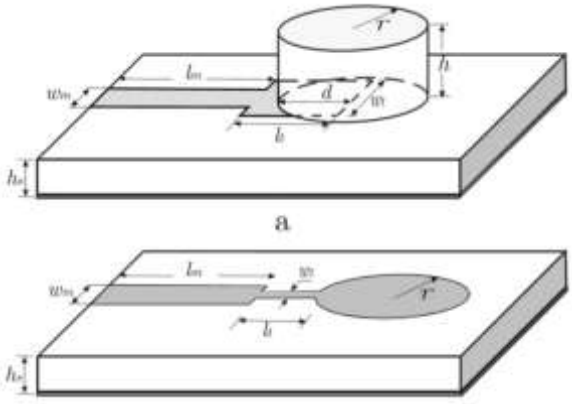

Fig. 2.2 Cylindrical DRA and circular disk microstrip antenna configuration [23].

Unfortunately, DRAs are more complicated to fabricate and costly when it comes to multilayer antennas and different feeding mechanisms are integrated to obtain low-profile and low-cost antennas such as integrating SIW feeding mechanism to reduce feeding losses at high frequencies especially at mm-wave frequencies [23]. For instance, the gain achieved in [24] is 5.7 dB and 5.51 dB for transverse and longitudinal slot respectively at 36 GHz, as shown in Fig 2.2. Later, to increase the gain, an array antenna was proposed using 1 × 4 SIW power divider to minimize the feeding losses.

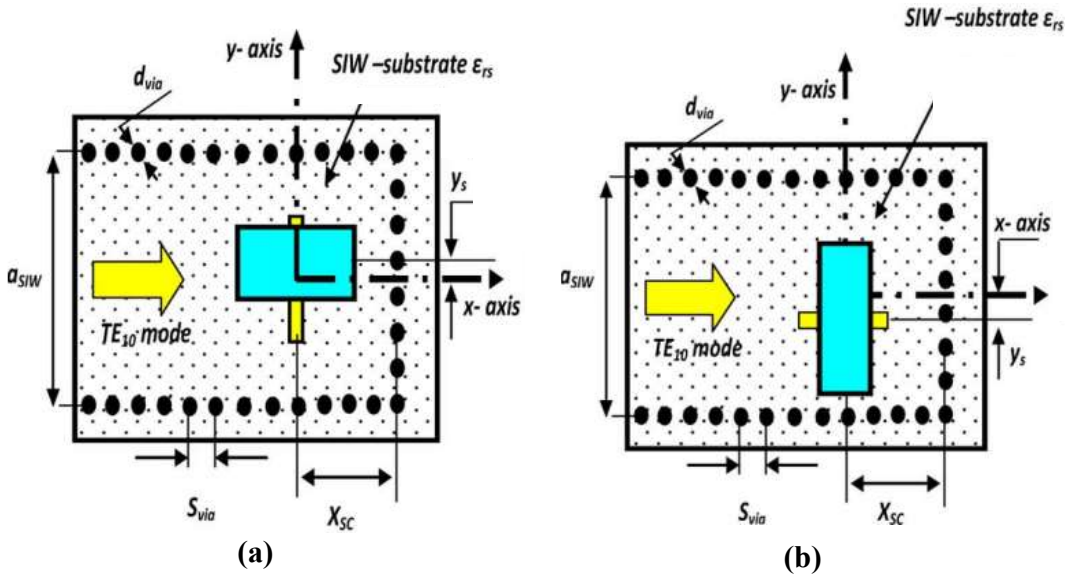

Fig. 2.3 SIW fed DRA using transverse and longitudinal slot at 36 GHz [24].

Therefore, it is understood that broadside antennas have a tendency to have low gain as compared to endfire antenna depending on the type of antenna used for either type of radiation. Such antennas need hybrid configuration such as DRAs, horn or lens, which are attached to the structure to enhance the impedance bandwidth and the overall gain of the antenna.

2.2.3 Substrate Integrated Waveguides (SIWs) Technology

, There has been development for high frequency integrated circuits called as substrate integrated circuits (SIC) to meet the requirements of wireless communications [25]. This technology is very beneficial in terms of integrating all circuits on a single substrate and/or multilayer platform. In simple words, we can say that dielectric based waveguides can be synthesized using air filled and metallized holes or vias with SIC technique that results in lower losses characteristics at high frequencies as compared to other conventional methods. The primary objective of SIC technology is to convert all non-planar structures into a planar form which allows easy fabrication procedure. Moreover, all other conventional transmission lines such as microstrip, coplanar waveguide (CPW), grounded coplanar waveguide (GCPW) can be integrated on a single substrate. A lot of study is done on transition between microstrip-SIW [26], CPW-SIW [27], GCPW-SIW [28], as shown in Fig 2.4, in order to have benefits of this technology. These transitions can be used to improve impedance matching in SIW based antennas.

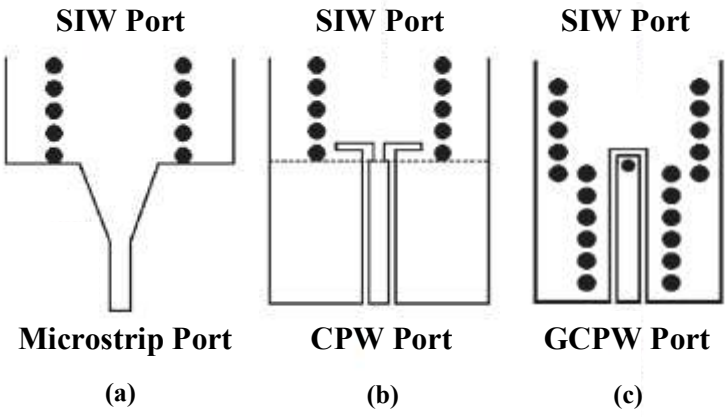

Fig. 2.4 (a) MS-SIW transition [26] (b) CPW-SIW transition [27] (c) GCPW-SIW transition [28]

SIW based antennas are very useful at millimeter wave frequencies as these antennas possess low attenuation losses. For instance, as shown in Fig 2.5, a high gain circular polarized SIW based millimeter wave antenna is presented in [29], which has x shaped slot to achieve circular polarization at 36.5 GHz.

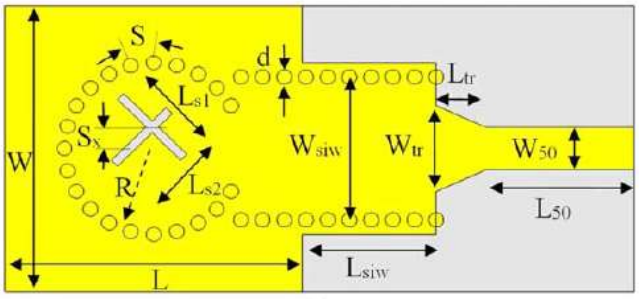

Fig. 2.5 Schematic diagram of circular polarized SIW based MMW antenna. [29]

2.2.4 Tapered Slot Antennas

Tapered Slot Antennas is one of the most widely used type of antenna that fulfills most of the current wireless systems requirements. These are also called Vivaldi antenna (traveling wave antennas) and it has advantages such as wide bandwidth, narrow beamwidth, and small physical structure. In general, TSA includes a tapered slot that is etched in the metallization on the dielectric substrate that is widen through its entire length to generate endfire radiation. The different shapes such as Vivaldi (exponential taper), LTSA (Linear TSA), ALTSA (Antipodal linear TSA), AFLTSA (Antipodal Fermi linear TSA) and DVLTSA (Dual V-type linear TSA) [30] can be illustrated in Fig 2.6.

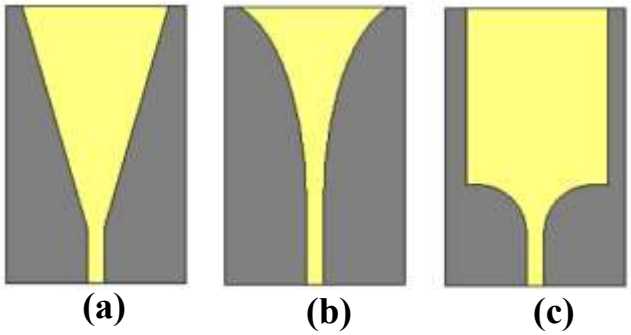

Fig. 2.6 (a) Linearly tapered slot antenna (LTSA) [30] (b) Exponentially tapered slot antenna (Vivaldi) [30] (c) Constant width slot antenna [30]

When we talk about Vivaldi antenna, the edge separation must be greater than half of the wavelength for traveling waves to flow at desired frequency. If the width of tapered slot decreases, the energy needed for traveling wave is more and the radiation is bounded by this width, whereas when the width is increased, there exists a weak energy in traveling wave and there is smooth radiation. The gain of such type of antenna is directly proportional to the length of antenna and ranges between $3\lambda_o$ and $8\lambda_o$ [31].

There is a lot of work done in last two decades on different types of tapered slot antennas using different feeding mechanisms in different frequency ranges. But we will discuss only those, which were done for millimeter wave applications and possessed high gain and wide bandwidth. For example, a wide bandwidth and 17 dB gain antipodal fermi tapered slot antenna with sine corrugation at 30 GHz, as shown in Fig 2.7, is presented in [32].

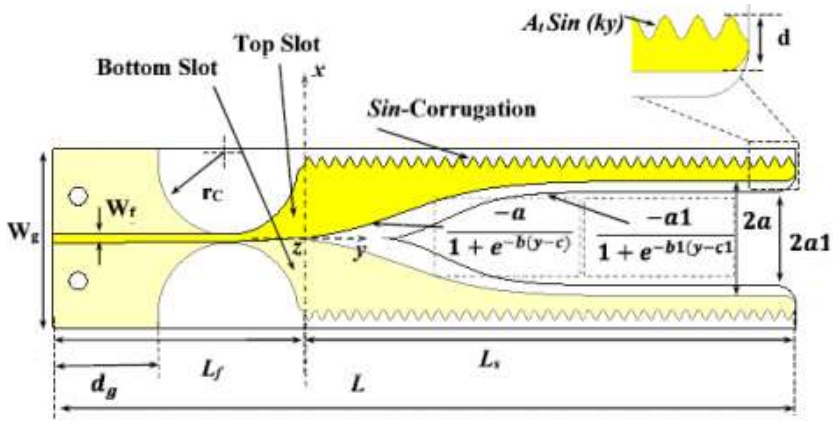

Fig. 2.7 Antipodal fermi tapered slot antenna with sine corrugation [32].

The taper curve is formed from Fermi-Dirac equation [33], given by

$$y = \frac{a}{1 - e^{-b(x-c)}}$$

This configuration of the antenna is designed using Fermi-Dirac equation and is a good candidate for high gain with wide bandwidth to cover the operational frequency band. Another good example of such type of antenna is tapered slot dielectric loaded antenna. In [34], an efficient planar dielectric loaded antenna for ultra-wideband wireless services for E and W bands (70-110 GHz) is presented as shown in Fig 2.8 (a). This paper compared two types of dielectric loading slab such as elliptical and rectangular dielectric loaded ALTSA with simple ALTSA antenna and ALTSA horn antenna. The measured gain is 14 ± 0.5 dBi with an efficiency of 84.23 % at 80 GHz. It also achieved 19 ± 1 dBi for its 1 × 4 array antenna with the wide bandwidth of the antenna.

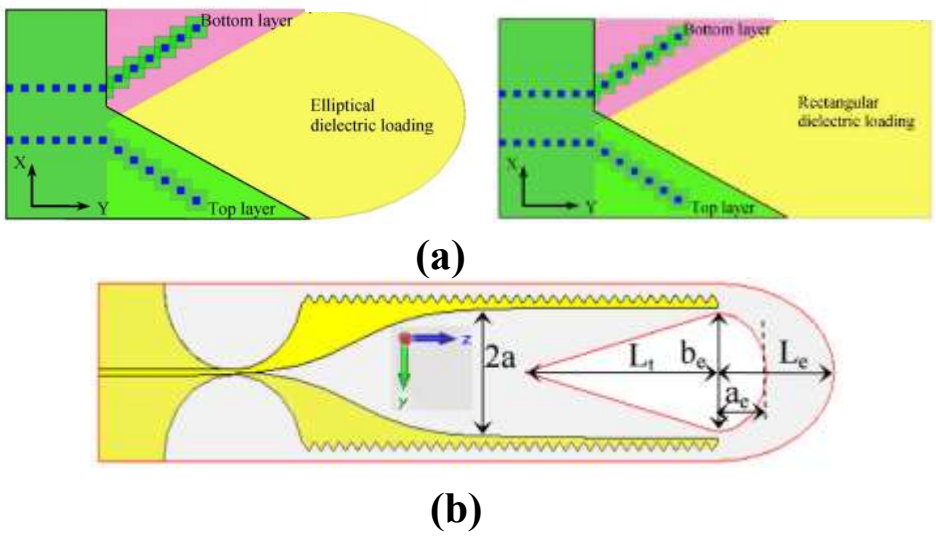

Fig. 2.8 (a) Elliptical and rectangular dielectric loaded ALTSA [34]. (b) AFTSA dielectric loaded configuration with sine corrugation [35].

Whereas in [35], an AFTSA with a diamond-shaped slot with dielectric loading on RO4003 substrate, as shown in Fig 2.8 (b), possess high gain of 20 dB at 60 GHz, which is better in both reflection coefficient and gain than unloaded AFTSA. There was an increase of gain by 1.5 dB by using this dielectric loading.

2.3 MMW technology based array systems

Recently there has been urgent need of array configurable antennas for wireless communications, which can provide control over radiated beam at different beam scan angles, unlike single antenna element whose radiation direction is fixed in a particular direction. Moreover, an array system can result in a high gain by using multiple antenna elements [36]. There exist different techniques to achieve this important characteristic of changing the radiation pattern such as the use of varactors, RF MEMS switches, phase shifters and developing the reconfigurable antenna structure with SIC technology. It can

be employed for applications such as satellite communications, wireless communication, imaging and detection of hidden objects and also in medical applications. The conventional array systems are microstrip based feeding array structures such as series feed network or corporate fed network [37], as shown in Fig 2.9.

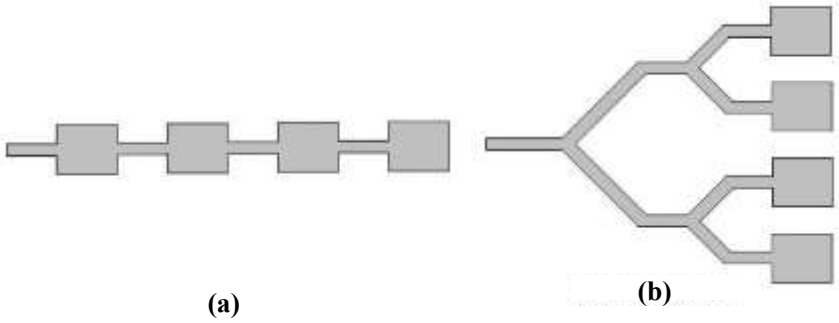

Fig. 2.9 (a) Series fed array structure [37] (b) Corporate fed array structure [37]

The primary advantage of microstrip array structure is the simplicity of array construction which can lead to compact and low-cost antenna array. But microstrip or hybrid array antennas face a lot of problems when it comes to the mm-wave frequency range. The losses (dielectric and conductor) are serious issue of concern in this frequency range and can affect radiation pattern that leads to decrease in total gain. In such scenario, broadside arrays can result in low gain due to high losses; therefore, it is recommended to use endfire high gain antennas usually between ~15-20 dB and that can still achieve high gain when constructed in array systems [37]. Therefore, in order to work with array systems for high gain and reconfigurable antennas, it is recommended to use substrate integrated waveguide technology which offers low insertion losses at milliliter wave applications. There is a lot of work already been done in millimeter wave antenna arrays and we will discuss some of the work related to SIW based antenna array at Ka band.

As said above, the losses increase with an increase in frequency for microstrip array system. For instance, in [38] as shown in Fig 2.10, the single element antenna has a gain of 2.5 dB (without corrugations) and 6.5 dB (with corrugations) in E-plane. Whereas, for eight element array without corrugations, it has a gain of 11 dB with a loss of 3.5 dB, which is a lot in terms of achieving the desired array gain (which is supposed to be 2.5+12=14.5 dB).

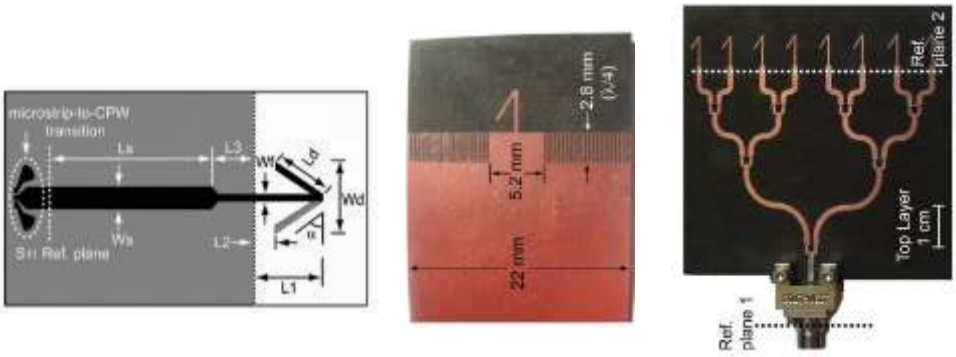

Fig. 2.10 Angle dipole antenna (without and with corrugations) and 1 × 8 element array [38]

In order to analyze SIW based power divider, we can see a 1 × 8 parallel SIW power divider in Fig 2.11 (a) [39] and 1 × 4 series fed array structure for Ka-band (at 36 GHz) in Fig 2.11 (b) [40]. Their single element had a gain of 5.7 dB (transverse slot) and 5.5 dB (longitudinal) and was able to achieve a gain of 14.8 dB for 1 × 8 antenna array and 11.7 dB (transverse slot) and 10.6 dB (longitudinal slot) for 1 × 4 antenna array respectively. The losses for SIW fed antenna array is minimal as compared to microstrip based array systems.

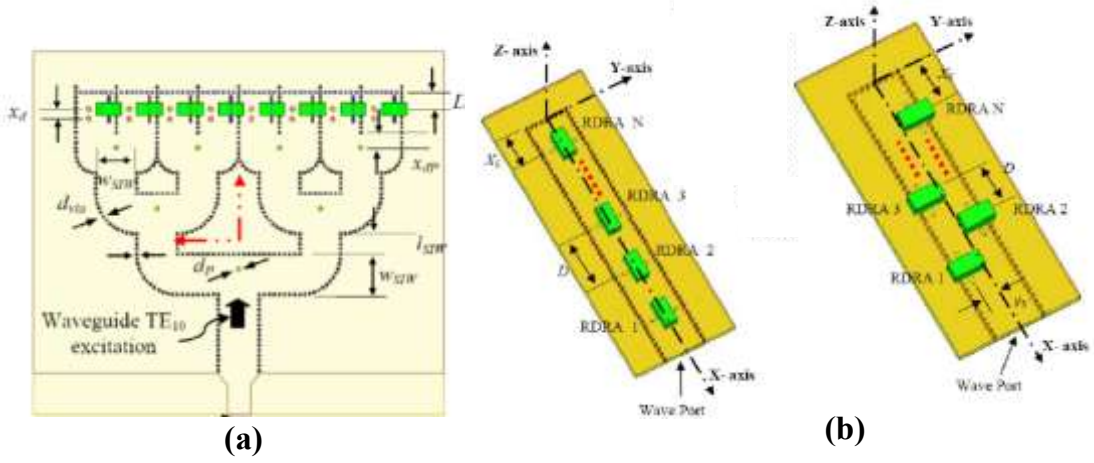

Fig. 2.11 (a) SIW 1 × 8 power divider for longitudinal slot based DRA [39] (b) Series fed array structure for transverse and longitudinal DRA [40]

2.4 MMW technology based beamforming systems

Nowadays, there has been tremendous interest in multibeam antennas for satellite and mobile communications, and multiple target radar applications. Beamforming networks (BFNs) are realized for multibeam antennas, and it is vital to decide with which type of transmission line, BFN can be realized. Previously the work was done with conventional techniques such as microstrip, coplanar waveguide, etc., but substrate integrated circuits are very beneficial for achieving low loss beamforming networks at high frequencies especially at millimeter wave applications [41]. Also, it is important to achieve high gain and high-efficiency multibeam antennas which have different implementation levels to achieve the same objective that is the beam rotation of antenna with desired gain and beamwidth. In this literature review, we will discuss beamforming antennas operated at Ka-band (26.5 GHz – 40 GHz).

In the context of beam rotation, the arrays can be classified into three categories: fixed directional beam antennas, electrically and mechanically steered beam antenna. The fixed directional beam antenna is the easiest configuration from all of them to achieve high gain, whereas electrically and mechanically steered beam is more complicated but can achieve much narrower beam than the conventional technique. The fixed directional beam antenna can be achieved by using phase shifters and for aperture coupled array, the size of an aperture can change the direction of beam easily but not in high beam scanning angles [38]. On the other hand, an electronically controlled switch for array elements can be used to reconfigure the beam direction in different scan angles. For example, as shown in Fig 2.12 (a) [42], each element is connected to the ground via a switch that has two states: 'ON' (when element is connected to the ground) and 'OFF' (disconnected from ground). The beamforming is performed using pin diode switches between element and ground with a suitable switching time. Also, in Fig 2.12 (b) [43], a reconfigurable four element patch antenna is presented using two bit digital pin diode phase shifters (digital phase shifters). Digital phase shifter is capable of realizing different phase shifts depending on the number of bits used, for instance in this case two bits are used which implies that there are four phase states (90°-360°).

There is another technique which can be useful to understand the beamforming concept for millimeter wave applications i.e. Beamforming networks (BFN) to avoid complex fabrication cost for beamforming antennas. BFNs are very useful for satellite and radar communications but are increasing in both complexity and variety of technologies used for multi-beam antenna systems.

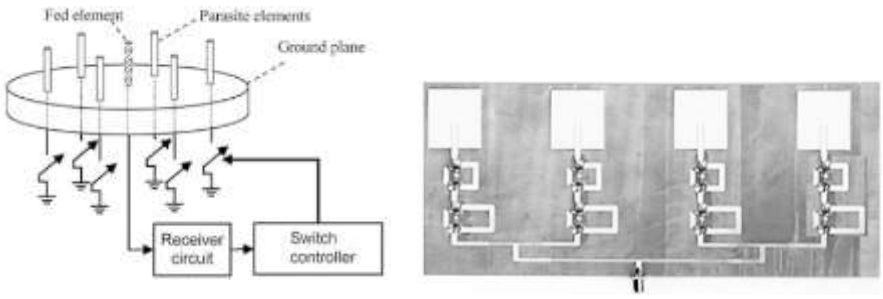

(a) **(b)**

Fig. 2.11 (a) Electronically switchable parasitic element array [42] (b) Four element array with patch elements and pin diode phase shifters [43].

For instance, for mobile satellite communications, the receivers have wide beamwidth with low antenna gain, on the other hand, for satellite earth station, there is need for a high gain antennas along with high mobility of the airplane [44]. But at millimeter frequency band, narrow beamwidth can be obtained as the wavelength is small, which can be beneficial to a greater resolution with a precision of target tracking, detection applications. It is found that the antenna configuration should be compact and simple to implement to achieve the desired results for millimeter wave applications. There has been tremendous work done including innovative feeding mechanisms made of SIW techniques, which shows better flexibility and design techniques. In [45], we can see in Fig 2.13 (a) that there is a meandering long slot leaky-wave antenna at millimeter wave frequency band (35 GHz). There are two types of configurations used in this paper: meandering long slot and meandering sidewall. The bandwidth (S_{11}≤-10 dB) of this antenna ranges between 33-37 GHz and the type 1 possess a gain of 12.2 dB with SLL of -27.7 dB along with 3 dB beamwidth of 14.2° in the beam direction at -38.1°. whereas type 2 has a gain of 12.7 dB with SLL of -29.3 dB along with 3 dB beamwidth of 13.9° in the beam direction at -37.9°. The beam scan angle for type 1 and type 2 varies from -26.9° to -45.8° and -27.1° to -45.7°

between 33-37 GHz respectively. This design has beam rotated in a fixed direction, and the beam is steered at different frequencies with improved cross polar level. Another example is illustrated in Fig 2.13 (b) [46] as half mode SIW quadri-polarization frequency scanning antenna. The antenna is designed using 3 dB directional coupler and two leaky wave antennas with -45° and 45° radiating slots. Changing the port excitation (changing the propagation direction of leaky-wave) can tilt the beam in opposite directions. The gain achieved in this antenna is 11.5-13.5 dB (port 1) and 12.5-14.85 dB (port 3) with beam direction ranging from -30° to +30° for frequencies between 33-39 GHz.

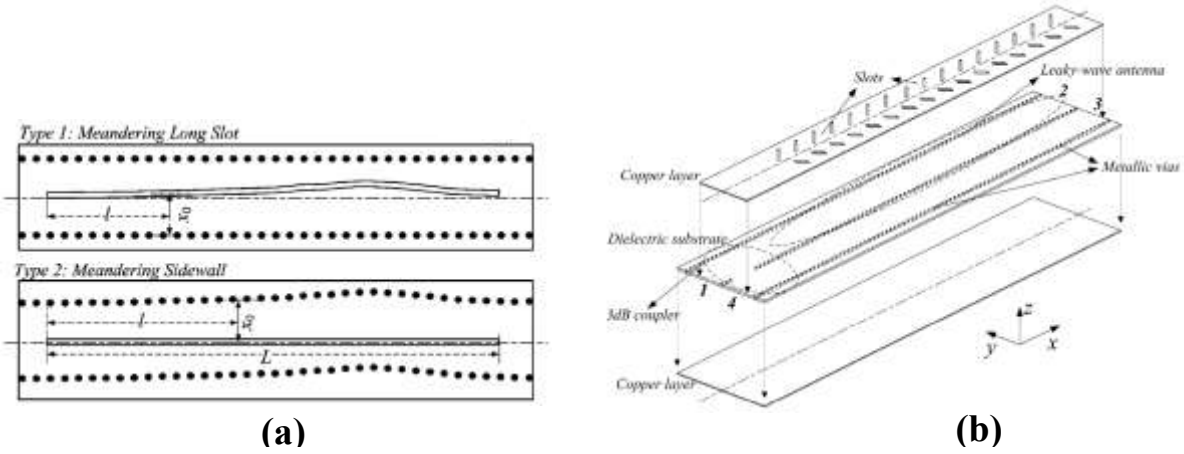

Fig. 2.13 (a) SIW long slot leaky-wave antenna [45] (b) Half mode SIW quadri-polarization frequency scanning antenna [46].

The previous two examples had beamforming at different frequencies as there was only one excitation port. It is possible to radiate beam steered at different beam scanning angles at one frequency but with a help of using multiple port propagation. For instance, 15 input ports and 11 array output ports structure are designed using SIW Rotman lens for 28.5 GHz as shown in Fig 2.14 (a) [44]. So each port is excited at one time, not simultaneously, to scan the beam at one frequency. This antenna (SIW slot array along with feeding SIW

Rotman lens) has a return loss below -15 dB with gain between 13.8-15.8 dBi with beam direction ranging between -40° to 40° with 3 dB beam widths between 14° to 22° for ports B1-B7. The dummy ports are designed to avoid high side lobe levels with radiation efficiencies between 19.8-56.4%.

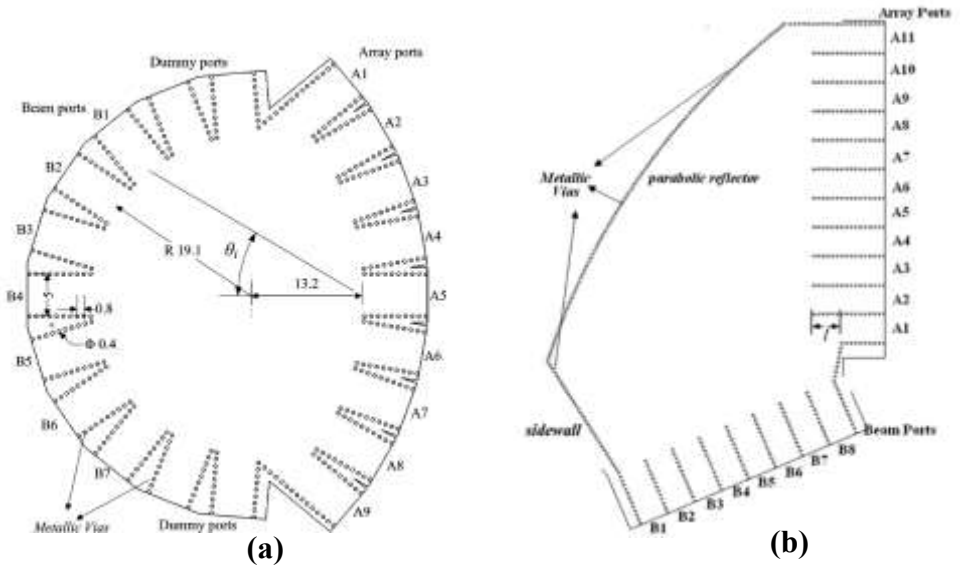

Figure 2.14 (a) SIW Rotman lens configuration [44] (b) SIW based parabolic reflector antenna [47].

In Fig 2.14 (b) [47], we can see another concept (known as SIW parabolic reflector concept) of using multiple beam ports. In order to eliminate the weakness of using the phase shifters and without moving the reflector mechanically the beam can be steered over an angle by moving the excitation feed from the parabolic focal point($y^2 = 4fx$). This antenna (same as used for Rotman lens) has a return loss below -15 dB at the center frequency of 37.5 GHz for all beam ports with gain in E-plane between 15.8-19.1 dBi and beam direction ranging between -30° to 30° with 3 dB beam widths between 7° to 10.6° for ports B2-B8. The radiation efficiencies vary between 21.5%-45.9%.

2.5 Summary

In this chapter, we have reviewed the state of the art of millimeter wave communications and type of antennas used for millimeter wave frequency range especially for Ka-band. Firstly, we have discussed two types of antennas: endfire and broadside radiation based antennas and we found that it is easy to design a single endfire antenna with a high gain and wide bandwidth. Then, the review of millimeter wave array systems and beamforming networks including MIMO is studied. Substrate integrated waveguide technology is more suitable than conventional planar transmission line such as microstrip for this frequency range in terms of low feeding losses, especially for antenna array structures. The literature review can be summarized in Table 2.1.

Table 2.1: Comparison of different antenna configurations

Antenna Structure	Radiation	Gain	Losses	Fabrication
Microstrip antennas	Broadside	Low	Low	Easy
	Endfire	High		
Dielectric Resonator Antennas	Broadside	Low	Low	Moderate
Substrate Integrate Circuits	Broadside	Low	Low	Moderate
	Endfire	High		
Tapered slot antennas	Endfire	High	Low	Easy
MMW microstrip array	Broadside	Moderate	High	Moderate
	Endfire	High		
MMW SIW array	Broadside	Moderate	Low	Moderate
	Endfire	High		
SIW Leaky wave antenna [45]	Broadside	High	Moderate	Moderate
HMSIW frequency scanning antenna [46]	Broadside	High	Moderate	Moderate
SIW Rotman lens slot array [44]	Broadside	High	Moderate	Difficult
SIW parabolic reflector array [47]	Broadside	High	Moderate	Difficult

The results of beamforming examples are tabulated in Table 2.2 in terms of their scan angle, beamwidth and gain capability.

Table 2.2: Comparison of different beamforming network configurations

Antenna Structure	**Scan Angle**	**Gain (dB)**	**Beamwidth**	**Efficiency**
SIW Leaky wave antenna [45]	-27° to -46°	12.2-12.7	12.7°- 14.2°	Moderate
HMSIW frequency scanning antenna [46]	-30° to 30°	11.5-14.85	4.2°- 7.4°	Moderate
SIW Rotman lens slot array [44]	-40° to 40°	13.8-15.8	14°- 22°	Moderate
SIW parabolic reflector array [47]	-30° to 30°	15.8-19.1	7°- 10.6°	Moderate

As we can see that a lot of beamforming networks are implemented for broadside radiation, therefore this thesis' main focus will be on endfire radiation based antenna array and beamforming networks.

Chapter 3: Research Methodology

3.1 Introduction

This chapter will focus mainly on the theoretical knowledge required to design high gain endfire antenna arrays and beamforming networks for millimeter wave applications. Firstly, we will discuss the basic antenna parameters that determines the antenna performance and are considerably important for antenna designing in two simulation tools being used i.e. CST Microwave Studio and Ansys HFSS. The results obtained from these two tools are well efficient to analyze the measured results. The numerical techniques for full wave analysis are discussed in this chapter as both the simulation tools are based on FEM (HFSS) and FIT (CST) algorithms respectively, which are suitable for homogeneous and inhomogeneous materials at millimeter wave frequencies.

The research methodology used in this thesis is explained in this chapter including the substrate integrated waveguide design, the design of single element antenna (Antipodal Fermi Linear Tapered Slot Antenna) and its parametric study for investigating their effects on the performance of the antenna. Then the design of SIW power divider and its comparison with conventional power dividers will be discussed in this chapter along with the beamforming techniques which will be used for designing endfire beamforming antenna subarrays.

3.2 Electromagnetic Analysis and Antenna Theory

3.2.1 Maxwell equations

The understanding of electromagnetic fields and waves including the radiated fields and scattering matrix is crucial in designing both types of antennas (endfire and broadside). All the work, which is studied and implemented such as single element antenna design, feed networks, and subarray structures are designed on simulation tools which are based on Maxwell equations. Solutions of Maxwell equations explains the electromagnetics related to different antenna structures and configurations operating at different frequency bands. The Maxwell equations can be expressed in either differential or integral forms [48] where $\vec{E}$ (V/m) and $\vec{H}$ (A/m) are electric and magnetic field intensities and $\vec{D}$ (C/m^2) and $\vec{B}$ (Wb/m^2) are electric and magnetic flux densities. $\vec{J_\iota}$, $\vec{J_c}$ (A/m^2) are impressed and conduction electric current density along with $\vec{\mu_\iota}$ (V/m^2), which is magnetic current density.

Differential form	**Integral form**	
$\nabla \cdot \vec{D} = q_{ev}$	$\oiint_S \vec{D} \cdot \vec{ds} = \zeta_e$	(3.1)
$\nabla \cdot \vec{B} = q_{mv}$	$\oiint_S \vec{B} \cdot \vec{ds} = \zeta_m$	(3.2)
$\nabla \times \vec{E} = -\vec{\mu_\iota} - \frac{\partial \vec{B}}{\partial t}$	$\oint_C \vec{E} \cdot \vec{dl} = -\iint_S \vec{\mu_\iota} . \vec{ds} - \frac{\partial}{\partial t} \iint_S \vec{B} . \vec{ds}$	(3.3)
$\nabla \times \vec{H} = \vec{J_\iota} + \vec{J_c} + \frac{\partial \vec{D}}{\partial t}$	$\oint_C \vec{H} \cdot \vec{dl} = \iint_S \vec{J_\iota} . \vec{ds} + \iint_S \vec{J_c} . \vec{ds} + \frac{\partial}{\partial t} \iint_S \vec{D} . \vec{ds}$	(3.4)

Whereas other parameters are q_{ev} (C/m^3) and q_{mv} (Wb/m^3) as electric and magnetic charge densities. ζ_e and ζ_m present the total electric and magnetic charge. In cases where EM field is complex, numerical techniques should be used as an exact solution in a closed loop, which is difficult to obtain. Therefore, it is recommended to use software tools based on different numerical techniques to design, simulate and optimize the design parameters before finalizing it for the fabrication process. It is also recommended to use different software based on different numerical techniques to have more precise and accurate measured results when compared with simulated results.

The solution of Maxwell equation is unique and valid for different antenna configurations when their boundary conditions are satisfied in terms of their electrical and magnetic surface current. The boundary conditions for the general case [48], perfect electric conductor (PEC) and perfect magnetic conductor (PMC) cases are shown in Fig 3.1, and their equations are tabulated in Table 3.1.

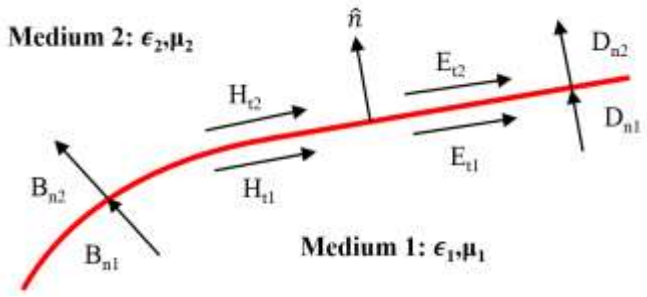

Fig. 3.1 Boundary conditions illustration for two mediums

Table 3.1: Electromagnetic boundary conditions summary [48]

Boundary condition type	Boundary equations	Analogous
General General equations for two mediums having different relative permittivity and relative permeability	$\hat{n} \times (\overrightarrow{H_2} - \overrightarrow{H_1}) = \overrightarrow{J_s}$ $-\hat{n} \times (\overrightarrow{E_2} - \overrightarrow{E_1}) = \overrightarrow{\mu_s}$ $\hat{n} \cdot \left(\overrightarrow{D_2} - \overrightarrow{D_1}\right) = q_{es}$ $\hat{n} \cdot (\overrightarrow{B_2} - \overrightarrow{B_1}) = q_{ms}$	General expressions at arbitrary interface of materials and/or surface currents
Perfect Electric Conductor (PEC) ($\sigma \to \infty$) All field components must be zero inside the conducting region ($\overrightarrow{E_1} = \overrightarrow{H_1} = 0$) and tangential component of electric field is zero	$\hat{n} \times \overrightarrow{H_2} = \overrightarrow{J_s}$ $\hat{n} \times \overrightarrow{E_2} = 0$ $\hat{n} \cdot \overrightarrow{D_2} = q_{es}$ $\hat{n} \cdot \overrightarrow{B_2} = 0$	To relations between voltage and current at the end of a short circuited transmission line.
Perfect Magnetic Conductor (PMC) All field components must be zero inside the conducting region ($\overrightarrow{E_1} = \overrightarrow{H_1} = 0$) and tangential component of magnetic field is zero	$\hat{n} \times \overrightarrow{H_2} = 0$ $-\hat{n} \times \overrightarrow{E_2} = \overrightarrow{\mu_s}$ $\hat{n} \cdot \overrightarrow{D_2} = 0$ $\hat{n} \cdot \overrightarrow{B_2} = q_{ms}$	To relations between voltage and current at the end of an open circuited transmission line.

3.2.2 Numerical techniques

The usage of Maxwell equations leads to lengthy calculations when EM fields are complex. Therefore, different numerical techniques can be applied to compute the complicated electromagnetic fields. There are several numerical techniques such as Method of Moment (MoM), Finite Difference Time Domain (FDTD), Finite Element Method (FEM), Finite Integration Technique (FIT), Fast Multipole Method (FMM), Transmission Line Matrix (TLM) and Uniform Theory of Diffraction (UTD), which are used as per different antenna configurations [49]. Some of the numerical techniques such as FEM and MoM solve the

EM problems in the frequency domain while other techniques such as FDTD and FIT solve in the time domain. Here we will discuss three techniques (MoM, FEM, and FIT) with respect to software package being used for analyzing the antenna parameters in this thesis. **Method of moment** technique is most widely used RF computational technique and in this technique, the radiating/scattering structure is replaced by equivalent surface currents. This surface current is discretized into segments through which a matrix equation is derived representing the effect of every segment on every other segment. This concept is employed, for example, through FEKO to model of rectangular patch antenna on the grounded substrate at $\lambda_d/15$ discretization as shown in Fig 3.2 [50].

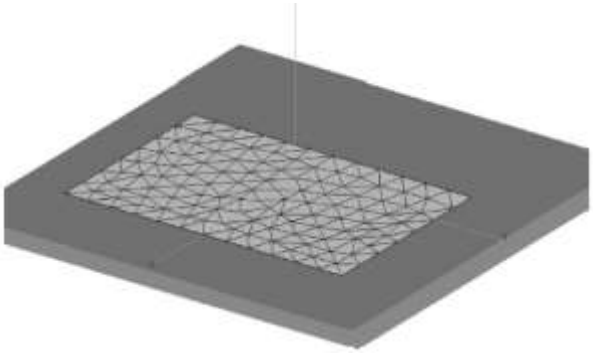

Fig. 3.2 FEKO model of a rectangular patch antenna on the grounded substrate at $\lambda_d/15$ discretization [50]

The advantages of this technique are as follows:

a) Perfectly or highly conducting surfaces are treated efficiently.
b) It incorporates the "radiation condition" automatically i.e. the correct behavior of the far field from the source.
c) The working variable is the current density from which antenna parameters can be derived such as impedance.

The disadvantages of this technique are as follows:

a) It is computing time and memory extensive to handle the electromagnetically penetrable materials.
b) It doesn't scale gracefully with frequency particularly when surface meshing is required.

3.2.2.1 Finite Element Method (FEM) for Ansys HFSS

This technique is one of the best-known methods using partial differential equations' solutions in applied mathematics and computational engineering. FEM may be derived from two viewpoints: variational analysis and weighted residuals. There are two types of meshes: triangular elements (surface meshes) and tetrahedron elements (volumetric meshes), which are used for discretizing the unknown structure. The fields can be calculated at nodes and approximated by interpolations on each finite element. There are various positive points for this numerical technique such as it is very flexible towards treating complex geometries and inhomogeneous materials. Also, this technique can handle dispersive materials, which are frequency dependent. Moreover, this technique can generate the symmetrical definite coefficient matrix from its algebraic equations and are also easy to define boundary condition as per antenna design requirements [50].

Some of the weak points of FEM are:

a) There is inefficient treatment of highly conducting radiators when compared to MoM.
b) FEM meshes can be very complex for large 3D structures.
c) Highly efficient iterative solvers are required when higher order elements are used.

Ansys HFSS uses finite element numerical methodology for generating EM fields' solutions for even complex structures. Firstly, the whole structure is divided into small

regions called elements. Then this software computes each element into finite element mesh (small 3D tetrahedral shapes) and assembling them with defined radiation boundary conditions and solving the whole system by a set of algebraic equations. The discretization optimization done by Ansys HFSS is very refined and provides more accuracy at edges, wave ports or even at discontinuities. Therefore, using less number of elements can speed up the simulation time but can lead to inaccurate results. As a conclusion, proper mesh refinement should be considered for obtaining accurate results. The steps for meshing for patch antenna are illustrated in Fig 3.3 [51], which shows discretization error being eliminated by refining the meshes.

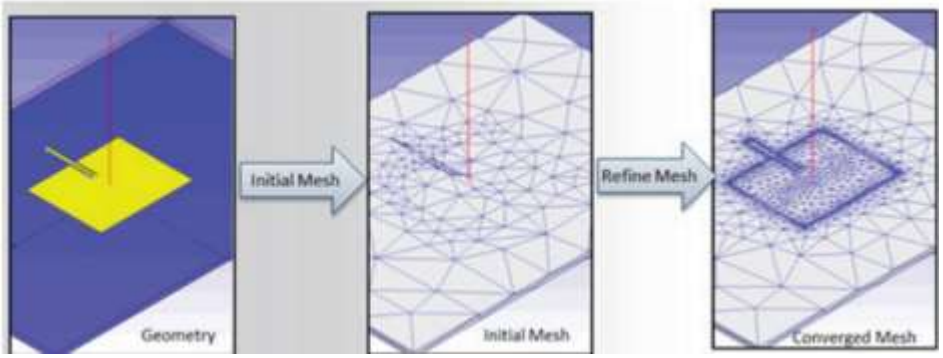

Fig. 3.3 Patch element mesh refinement stages (Initial mesh – Refine Mesh – Frequency Sweep) [51]

3.2.2.2 Finite Integration Technique (FIT) for CST Microwave Studio

This technique uses integral form of Maxwell equations for mesh refinement instead of partial differential equations as used in Finite Element (FE) method. This technique can be seen in Computer Simulation Technologies (CST) Microwave Studio software, which is very powerful and widely used 3D EM field simulator. This software has both time and frequency domain simulations, in which both hexahedron and tetrahedron types of meshes can be implemented. The electric and magnetic field vectors are computed in the time

domain at discrete spatial locations and at discrete time samples. The densely mesh can take more simulation time because the maximum step time used is dependent on minimum mesh step size which is determined by mesh density in the whole meshing process. Moreover, after the spatial meshing or discretization, FIT is implemented, in which integral form of Maxwell equations are converted into a set of discrete matrix equations [52].

3.2.2.3 Analysis of Tapered Slot Antenna using FEM (HFSS) and FIT (CST)

The antenna used in this thesis is one of the forms of the tapered slot antenna i.e. antipodal fermi linear tapered slot antenna (AFLTSA), whose design details are discussed in the following section. This antenna is simulated in both the simulating tools and mesh refinement is analyzed to obtain similar results, not exact ones as both of them uses different numerical techniques. It is considered that for single mode antenna such as broadside patch antenna, it is possible to get similar s-parameters in both the software but antennas which are multi-TEM modes such as tapered slot antenna, s-parameter results can vary. This variation happens because TSA has multimode effects, especially at millimeter wave frequency band; therefore it is interesting to analysis two different numerical techniques for AFLTSA.

Firstly, for AFLTSA, the meshing is analyzed in HFSS, as shown in Fig. 3.4, which uses frequency domain and have small tetrahedral shapes for meshing. The thick and thin meshing can be seen in this type of antenna.

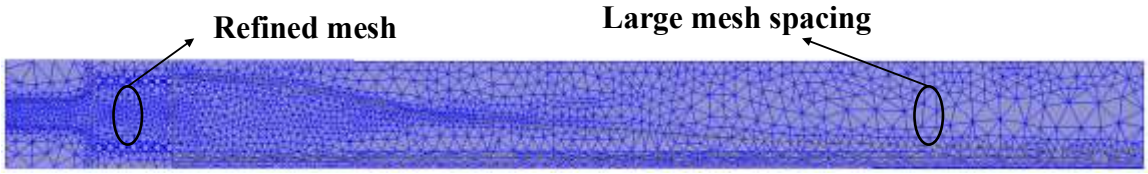

Fig. 3.4 AFLTSA meshing in Ansys HFSS using Finite Element Method.

Furthermore, the AFLTSA is meshed in CST in the time domain with hexahedral mesh refinement and also in the frequency domain with tetrahedral meshing as shown in Fig. 3.5.

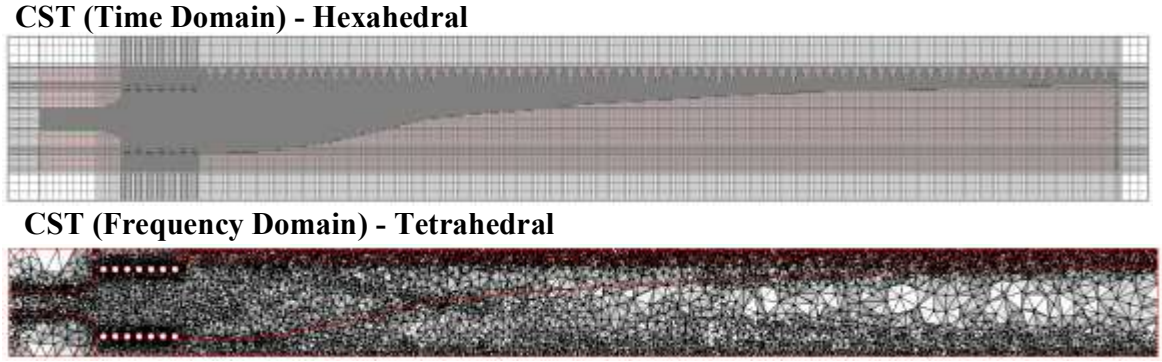

Fig. 3.5 AFLTSA meshing in CST Microwave Studio using Finite Integration Technique.

Both numerical techniques are suitable for designing antennas and can have different results (almost similar) but not exact ones. The case in which there similar results is valid in case of single mode antenna but for multi-mode antenna like TSAs, there is a probability that return loss shifts ups or down using FEM and FIT. Therefore, TSA should be designed in such a way that design specifications are analyzed parametrically in both the simulating tools and are suitable before proceeding with the fabrication process.

3.3 Substrate Integrated Waveguide (SIW)

The planar circuits such as microstrip, co-planer waveguide possess high conductor losses and high cross talk and transmission losses at high frequencies due to which the substrate integrated circuits (SICs) such as substrate integrated waveguide technology (SIW) is implemented [53], which offers low cost, high Q factor and low insertion loss at high frequencies and are very appropriate to construct millimeter wave integrated antennas and beamforming networks (BFN).

SIW is considered as feeding network along with microstrip transition for our work. SIW is made up of two rows of conducting cylinders (vias) or slots embedded in a dielectric substrate that connect two parallel metal plates [53]. The typical geometry of SIW structure is illustrated in Fig 3.6, where d is the diameter of via, s is spacing between two vias and wsiw is the width of SIW. As SIW exhibits propagation characteristics such as of the rectangular metallic waveguides, SIW modes have same modes as of the latter i.e. TE_{n0} modes. SIW doesn't support TM waves because of gaps between the metallic vias, which means TM fields determine longitudinal surface currents which are subject to a strong radiation due to presence of the gaps. Therefore, TE_{10} mode is the fundamental mode.

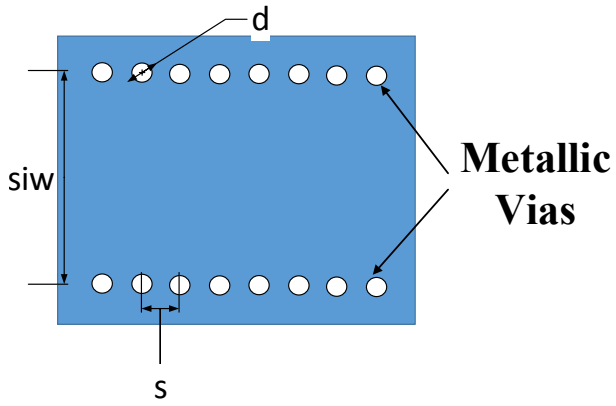

Fig. 3.6 A typical substrate integrated waveguide structure (top view)

The SIW design equations with respect to the conventional waveguide can be found in [54] as:

$$\overline{wsiw} = \zeta_1 + \frac{\zeta_2}{\frac{wsiw}{s} + \frac{\zeta_1 + \zeta_2 - \zeta_3}{\zeta_2 - \zeta_3}} \tag{3.5}$$

with equivalent waveguide width as $\mathbf{W_e = wsiw.\overline{wsiw}}$ and $\overline{\mathbf{wsiw}}$ is waveguide normalization factor.

Also the other constants can be calculated as:

$$\zeta_1 = 1.0198 + \frac{0.3465}{\frac{\text{wsiw}}{\text{s}} + 1.0684} \tag{3.6}$$

$$\zeta_2 = -0.1183 + \frac{1.2729}{\frac{\text{wsiw}}{\text{s}} - 1.2010} \tag{3.7}$$

$$\zeta_3 = -0.1183 + \frac{1.2729}{\frac{\text{wsiw}}{\text{s}} - 1.2010} \tag{3.8}$$

Two important factors that should be kept in mind while designing width of SIW feeding structure: diameter of vias (d) and spacing between them (s). In above equations, there is no provision of checking on radiation losses, but there are other conditions in equation 3.9 and 3.10, which ensures that there are no radiation losses due to EM field leakage in the SIW structure [55].

$$\text{d} \leq \frac{\lambda_g}{5} \qquad \text{s} \leq 2\text{d} \tag{3.9}$$

$$\text{wsiw} = 0.5 \times \left[W_{eq} + \sqrt{\left(W_{eq} + 0.54\text{d}\right)^2 - 0.4\text{d}^2} \right] + 0.27\text{d} \tag{3.10}$$

3.4 Antipodal Fermi Linear Tapered Slot Antenna (AFLTSA)

3.4.1 Introduction

The antenna used in this thesis is one of the types of the tapered slot antenna: antipodal fermi linear tapered slot antenna, as shown in Fig 3.7, which can be designed using Fermi Dirac equation as given in equation 3.11, where a, b, and c are constants which determine the slope, length, and width of the curve.

$$y = \frac{a}{1 - e^{-b(x-c)}} \tag{3.11}$$

The Fermi shaped tapered slot is flared on either side of the substrate in opposite direction to maximize the radiation in endfire direction. The coupling between SIW and the tapered slot is very important and the maximum electric field in SIW structure should be coupled into the tapered slot. As per equation 3.11, the Fermi distribution curve can be modified to maintain acceptable coupling between SIW and the tapered slot. An essential condition to generate radiation for Fermi Tapered Slot antenna is that its aperture width must be more than half the guided wavelength at the lowest cut off frequency and r to meet this condition, the length of the antenna increases, which has an effect in beam rotation for multimode beamforming networks.

There is a use of corrugations in the design of this antenna. The corrugations can be rectangular [33], comb-shaped [56] or sinusoidal shape [32], which controls the surface waves on the side edges of the substrate. Moreover, sine shaped corrugation improves the radiation from sharp edges resulting in wider bandwidth and low side lobe levels (SLL). Thus, with a help of sine shaped corrugation, it is possible to enhance the radiation characteristics and return loss, and thus, decreasing SLL.

3.4.2 AFLTSA Design

The antenna, as shown in Fig 3.7, is designed on substrate Rogers 5880, with a relative dielectric permittivity ε_r=2.2 and a loss tangent tan δ = 0.0009 with 0.508 mm (20 mils) thickness for 32.5 GHz solution frequency. Firstly, the simulation and parametric study are carried out in Ansys HFSS and then was simulated with analyzing the antenna in CST Microwave Studio. The parameters for single element AFLTSA are tabulated in Table 3.2.

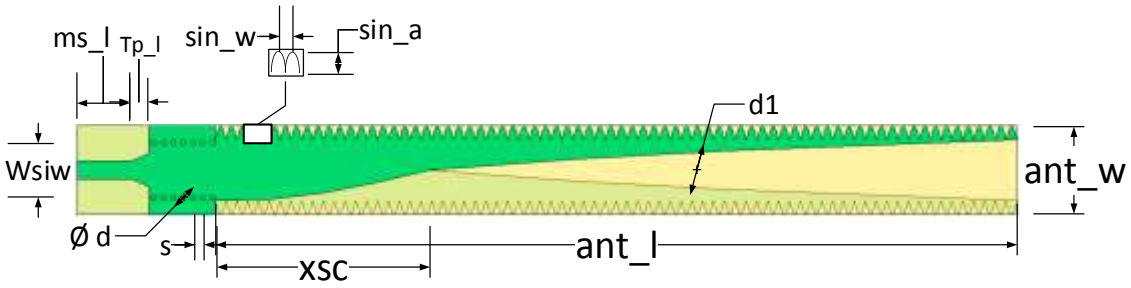

Fig. 3.7 Antipodal Fermi Linear Tapered Slot Antenna with sine corrugations and SIW-MS feeding technique.

Table3.2: Parameters of the proposed antenna.

Parameter	wsiw	ant_w	ant_l	xsc	ms_w	ms_l	d	s	sin_a	sin_w	d1
Value (mm)	5	8	74	19.8	1.61	5	0.5	0.9	1.25	1	1.98

AFLTSA can be divided into three transition mode parts with respect to their electric field distribution: microstrip to ground, SIW and tapered slot. These parts can be illustrated in Fig. 3.8 with their electric field direction indicating the change in field with different transitions.

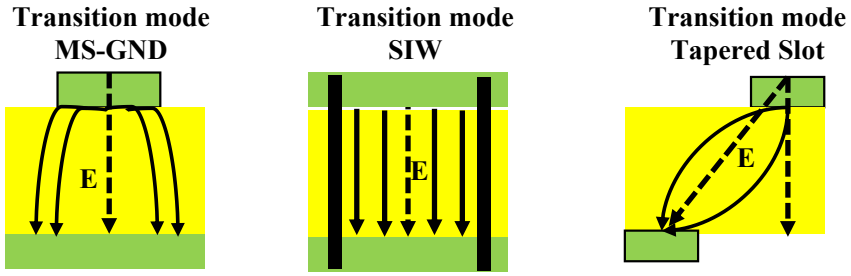

Fig. 3.8 AFLTSA Transition modes with respect to their electric field distribution

Effect of sine corrugations:

The sine corrugations are used in this antenna along its surface edges to have smooth surface waves along the edges, thus helping in improving radiation characteristics of the

antenna. This phenomenon can be explained through a study of AFLTSA with no corrugations, with rectangular corrugations and with sine corrugations. This study can be illustrated, as shown in Fig 3.9, through their electric field distributions and analyzing the effect of anti-phase waves, which is an important factor in determining the radiation properties of this antenna.

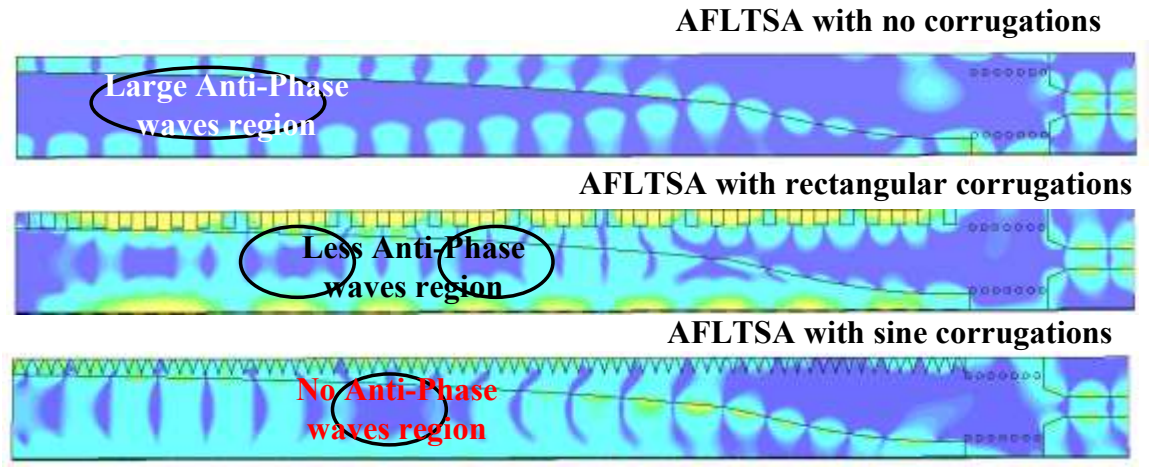

Fig. 3.9 AFLTSA electric field distribution for three corrugations profile (no corrugations, rectangular corrugations and sine shaped corrugations)

It is observed that the AFLTSA with no corrugations has a large anti-phase region and a high reflected wave back to the feeding line. The rectangular corrugations help in controlling the reflected waves but can't eliminate the antiphase region completely. The sine corrugation can eliminate antiphase waves completely with a small reflected wave and low loss at the surface edges. Therefore, sine-shaped corrugation creates a smooth behavior of the surface current distribution and reduces the effects of current disruption on the sharp angled edges.

3.4.3 Parametric Study

The parametric study is analyzed for two parameters which can have an effect on radiation pattern and return loss for this antenna: (a) tapered slot position (xsc) and (b) distance between the tapered slot curves on either side of substrate (d1).

A) **Tapered slot position (xsc):** The tapered slot position, denoted by xsc is investigated at multiple values of guided wavelength (λ_g=6.68 mm) i.e. *xsc = λ_g*n (for n=1, 2, 3…)* at which the antenna is operated. This distance can be controlled by adjusting a, b, and c constants of the Fermi-Dirac equation (3.11). In Fig 3.8 (a), it is seen that with an increase in the tapered slot position, there are more resonances with wider bandwidth (29-39 GHz) with an increase in total gain (from 6 dB at λ_g to 12.5 dB at 3λ_g @32.5 GHz). The increase in gain increases with the slot distance, which is due to improved coupling between SIW and tapered slot. It can be observed that the gain and return loss is worsened at shorter distances i.e. λ_g due to no coupling between SIW and tapered slot as most of the power is reflected back to the excitation input port.

B) **Distance between Fermi curves (d1):** The distance between Fermi curves on either side of the substrate is the distance between inner end points curve as shown in Fig 3.7. This parameter is also analyzed with respect to the guided wavelength, and we can see from Fig 3.8 (b) that the return loss is pretty much same with respect to the parametric change but there is an increase in total gain (~1 dB) with increase in d1 from 0.2λ_g - 0.5λ_g. However, this distance has a limit because of Fermi aperture width leading to increase in side lobe levels.

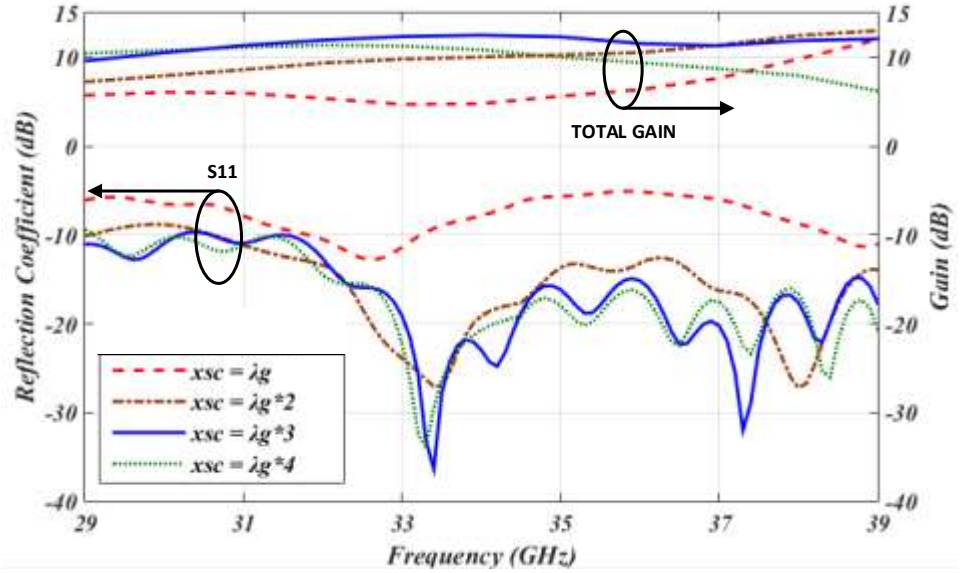

(a)

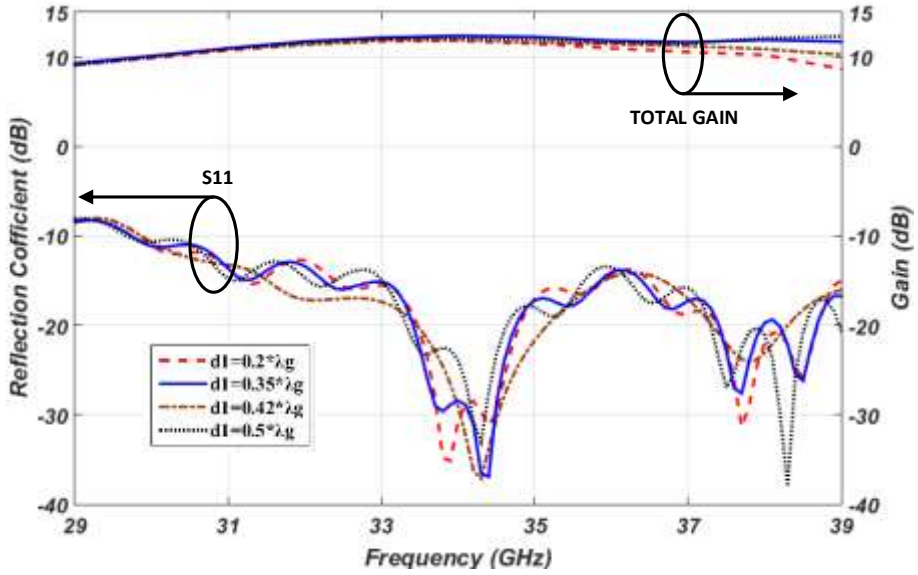

(b)

Fig. 3.8 Parametric analysis of AFLTSA by (a) Tapered slot position (xsc) and (b) Distance between the tapered slot curves on either side of substrate (d1).

Therefore using the analyzed parameters as tabulated in Table IV, the reflection coefficient is plotted in both the software tools with the total gain over the desired frequency range 29-

39 GHz. The reflection coefficient obtained is better than -15 dB with a wide bandwidth of more than 30% as shown in Fig 3.10 (a).

3.4.4 Radiation pattern characteristics

The succeeding important parameter to analyze is radiation pattern characteristics. The characteristics includes the total gain that this antenna can radiate and also side lobe levels it exhibits in E-plane and H-plane respectively. The E-plane and H-plane for AFLTSA endfire antenna are illustrated in Fig 3.9, which explains how both the planes for an endfire antenna are analyzed. The E plane is defined parallel to the feeding excitation, and H plane is as usual perpendicular to E-plane.

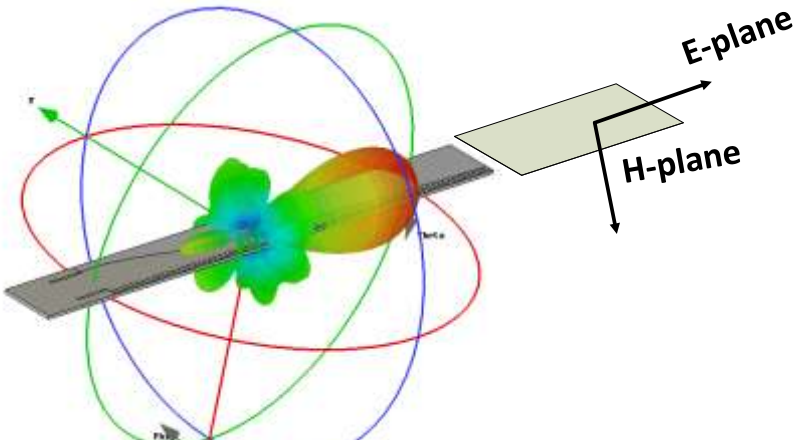

Fig. 3.9 E-plane and H-plane definition for AFLTSA

As shown in Fig 3.10 (b), the total gain obtained at 32.5 GHz in HFSS is 12.5 dB with SLL of -17.85 dB in both the planes. Also, the wide beamwidth achieved in E-plane and H-plane are 30° and 40.57° respectively. Whereas in CST, it is observed that a total gain of 12.6 dB with SLL better than 15 dB and beamwidths of 28° and 34 in both the planes are obtained respectively.

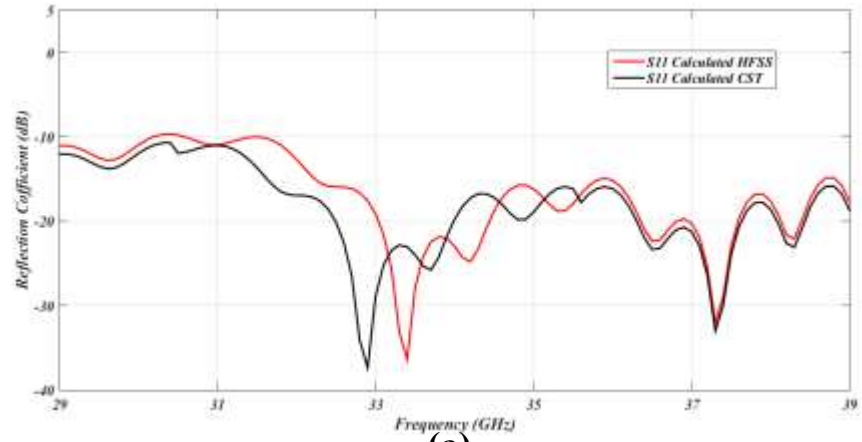

(a)

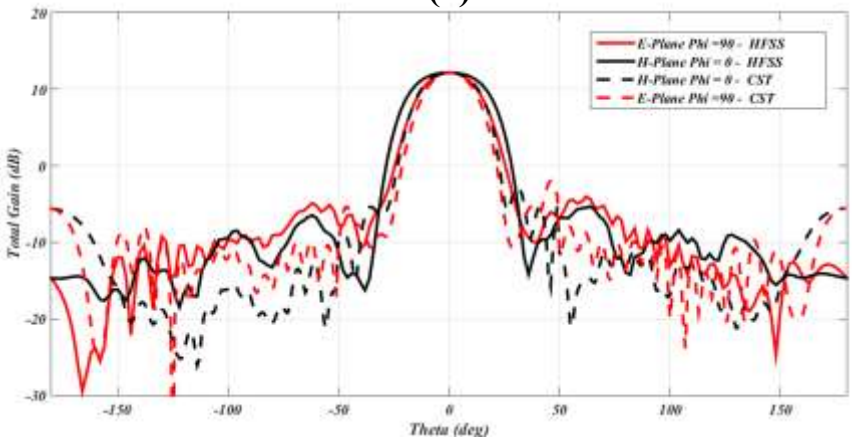

(b)

Fig. 3.10 (a) Reflection coefficient (S11) using HFSS and CST for AFLTSA (b) E-plane and H-plane rectangular radiation far field plot using HFSS and CST.

Overall, it is seen that using two different numerical techniques; multi-mode TEM tapered slot antenna is simulated and studied parametrically. This proposed antenna can achieve wide bandwidth and high gain with low side lobe level for millimeter wave applications. Therefore, our single element antenna is ready to be operated for large array and beamforming systems.

3.5 Substrate Integrated Waveguide Power Dividers

3.5.1 Introduction

The substrate integrated waveguide technology plays a major role in improving the quality of substrate integrated array systems at millimeter wave frequency band. The array systems, as discussed in the literature review, helps in increasing the gain with minimal losses for Ka-band applications. It is important to construct an array system which can have minimum losses that include conductor losses and dielectric losses. Although with the help of SIW power dividers, there is a possibility of having high gain antenna array structure and also with the help of techniques such as Dolph-Chebyshev, Taylor distribution, etc., we can obtain low side lobe levels.

The reduction in impedance bandwidth and increasing side lobe levels are two encountered problems while designing an array system, which can be overcome only by designing wide impedance bandwidth antenna with low side lobe levels. For instance, the antenna used here i.e. antipodal fermi linear tapered slot antenna has very wide bandwidth with high gain and low side lobe level as discussed in the previous section. Therefore by implementing a SIW power divider, a high gain antenna is possible with acceptable bandwidth and low side lobe levels (better than 20 dB).

3.5.2 Types of power dividers

There are different SIW power dividers which are studied for our work. The first one is parallel feeding divider that has a symmetrical configuration with equal transmission coefficients within a wide band. In parallel feeding network, there are two configurations: T-divider and Y-divider as shown in Fig. 3.11. In T-junction power divider, a metallized

adaptive via is implemented to achieve low return losses. The diameter and offset position of adaptive via helps in having a better matching between the input port and output ports [57]. For Y-divider, the width of input SIW and the distance between two discontinuities (l) can be optimized to achieve better matching and power division between input and output ports [58].

The modified Y-divider for W-band 16 way SIW parallel feeding divider is implemented in [59]. Y divider is chosen over T-junction divider as the latter has the relatively narrow bandwidth for such large array system.

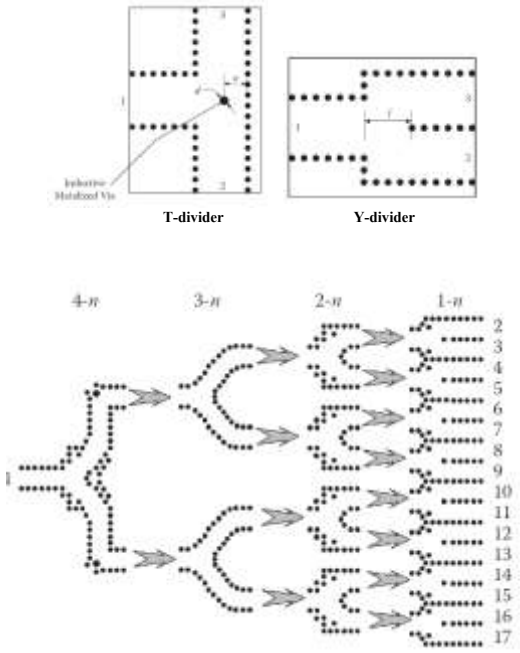

Fig. 3.11 T junction and Y junction SIW parallel feeding power divider [57]. W band SIW feeding power divider [59]

In this power divider, several stage two-way dividers are grouped to realize a 2^n-way large-scale divider as shown in Fig 3.11. In contrast to such complex structures, it is difficult to minimize the array system and these parallel feeding dividers generates high side lobe levels. In order to overcome parallel feeding power divider issues, another type of power

divider called as series feeding power divider as shown in Fig. 3.12 [59], is used. Such dividers also use adaptive vias based on techniques such as Dolph-Chebyshev or Taylor distributions, which are implemented to have compact size and low side lobe levels better than 20-30 dB.

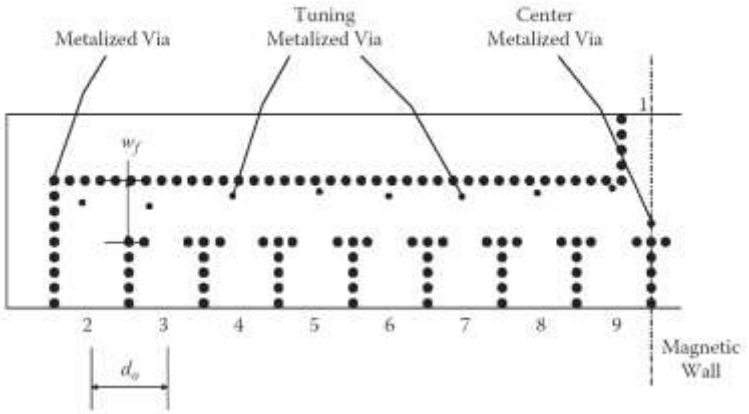

Fig. 3.12 Configuration of a half of the 16-way SIW series feeding divider [59].

Moreover, the design of SIW power divider for AFLTSA is explained in detailed in Chapter 4 with all the calculated results.

3.6 Substrate Integrated Waveguide Beamforming Networks

Multibeam antenna is considered to be one of the most effective method to increase the capacity and reduce power consumption for communication systems [60]. In the previous chapter, the literature review gives an overview of beamforming networks with SIW technology for millimeter wave applications in which we discussed analog and digital beamforming techniques. In this section, we will discuss some of the techniques used in performing beamforming for multibeam AFLTSA. There are two network flow models for multibeam antennas: Symmetrical model [60] and Asymmetrical model [61] as shown in Fig. 3.13.

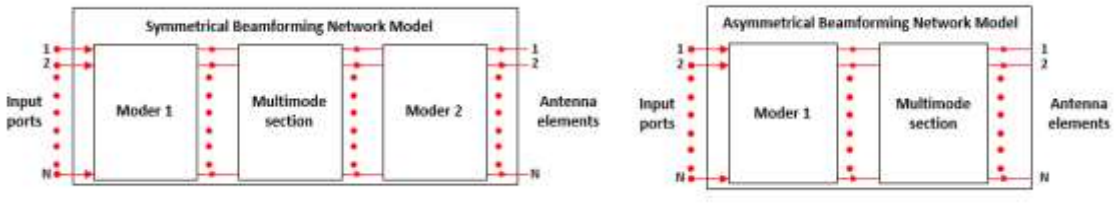

Fig. 3.13 Symmetrical and Asymmetrical network flow model for multibeam antenna design [61]

The common point for both the network models is that the number of input ports is equal to the number of antenna elements. Symmetrical model is more flexible with respect to antenna specifications but is less compact as compared to the asymmetrical model. In other words, we can only use an asymmetrical model, where the width of SIW is equal to the antenna width, whereas symmetrical model can be adjusted according to antenna width. In Fig. 3.13, Moder 1 and Moder 2 represent the field amplitude transformation, which can excite different modes within the multimode section while the multimode section is used to achieve and control phase transformation as the amplitude of each mode propagated is invariant with respect to the longitudinal direction. The design of multimode section is very important and sensitive for performing beamforming operation. The comparison between three multibeam antennas is illustrated to minimize the size of the antenna structure and also ease the fabrication process. The SIW Butler matrix shown in Fig 3.14 has a radiation efficiency less than multimode BFN (symmetric) due to its compact configuration [60]. On the other side, to improve the radiation efficiency, asymmetric multibeam BFN is presented in [61]. The multimode BFN is very efficient in comparison to Butler matrix as it has no 3 dB couplers, crossings, and fixed phase shifters, which will be difficult to miniaturize and fabricate. Also compared to Rotman lens [44] and parabolic reflector [47], it is easy to design and fabricate which decreases the overall design complexity.

We will be using symmetrical beamforming network with no phase shifters for our thesis' work, and the design methodology is explained in chapter 5.

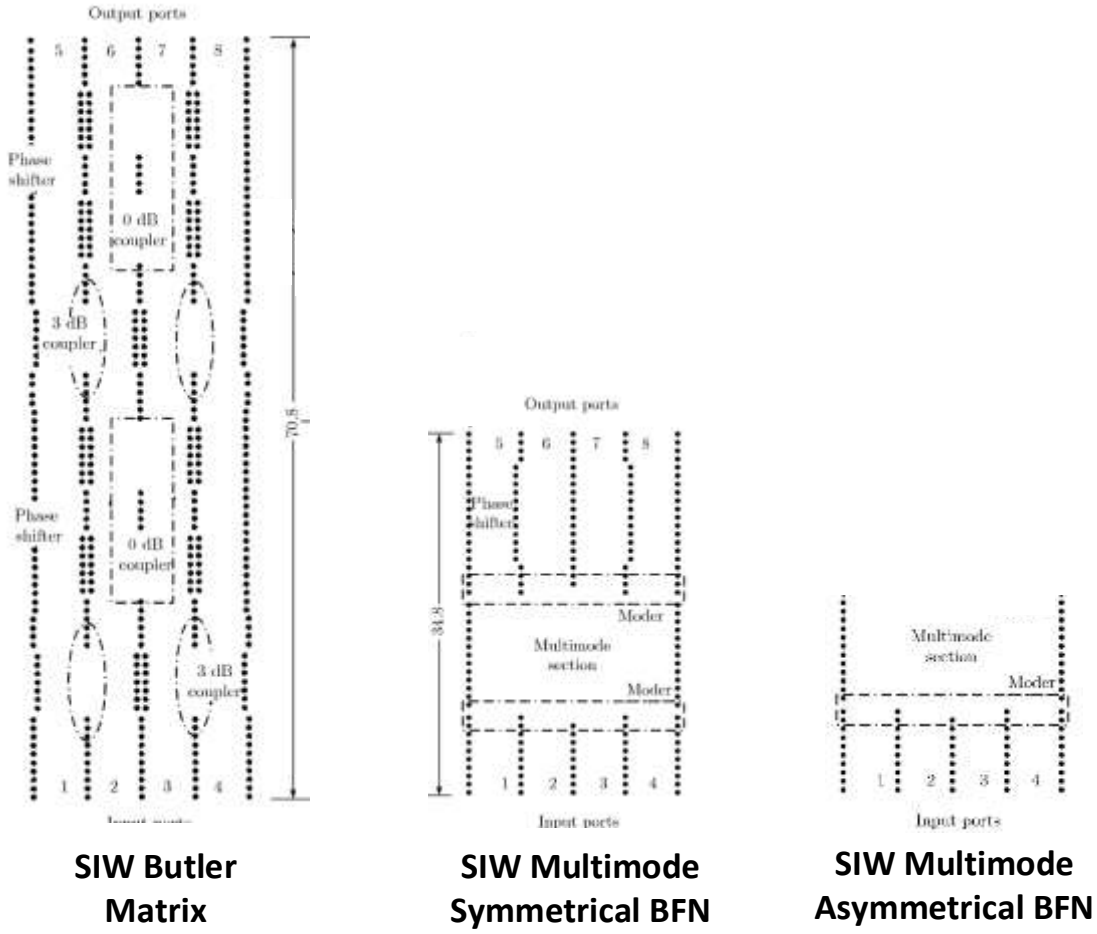

Fig. 3.14 Compactness of Butler matrix, Multimode BFN (symmetrical and asymmetrical) [62]

3.7 Summary

In this chapter, we have outlined the basics of electromagnetics including Maxwell equations with the suitable boundary conditions. The numerical techniques are briefly explained specifically Finite Element Method and Finite Integration Technique which are used by two commercial software, Ansys HFSS, and CST Microwave Studio, respectively. Later applications of these two techniques to AFLTSA are illustrated by several examples.

Furthermore, the design of SIW structure is explained along the design of single element AFLTSA. A parametric study is carried out to obtain wide impedance bandwidth and radiation characteristics for this antenna and also to achieve high gain and low side lobe in both the E-plane and H-plane. The design of single element is very useful as it helps to study its array and beamforming systems in following chapters.

An introduction to research methodology used for SIW power divider and beamforming networks is explained at the end of this chapter, which gives us a brief overview of arrays and BFNs. We will be using SIW series feeding network and symmetrical multimode BFN for our thesis' work.

Chapter 4: Antipodal Fermi Linear Tapered Slot Antenna Array

4.1 Introduction

The design of planar SIW based antipodal fermi linear tapered slot antenna is presented in this chapter to achieve a high gain, wide impedance bandwidth and low side lobe level. Such antenna configuration can be beneficial for 5G network applications including millimeter wave applications.

In this chapter, the design of 1 × 8 SIW power divider is presented with its results and discussion on return loss and in phase distribution for input and output ports. Later, the whole antenna structure is simulated using both software: HFSS and CST, which concludes the fabrication feasibility of such structure at MMW-band.

4.2 Design of 1 × 8 SIW power divider

The design of a series SIW power divider is analyzed for integration with high gain antenna structure. The discussion on designing of SIW power divider will be done in this section. This design is symmetrical series feeding network using Dolph-Chebyshev techniques with unequal power flow at each output port with respect to input port [62]. This method helps in achieving low side lobe levels and also minimizing the size of the power divider.

Fig. 4.1 presents the 1 × 8 SIW power divider which has one input port (port 1) and 8 output ports (port 2-9). The adaptive vias are implemented to obtain impedance matching and low SLL. As a result, there is an unequal power division that has some insertion losses

but is acceptable as SIW technique has the capability to generate low losses at high frequencies.

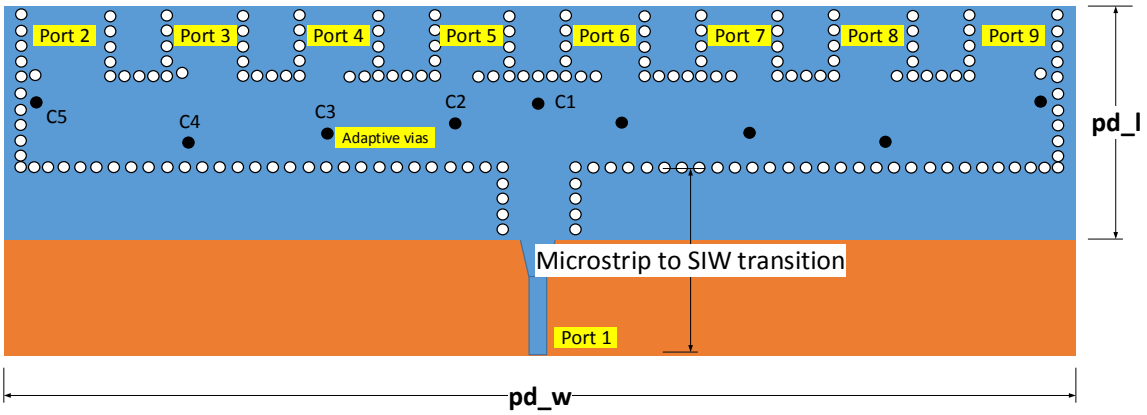

Fig. 4.1 1 × 8 SIW series feeding divider with MS-SIW transition.

The design of adaptive vias (C1-C5) is studied to have better impedance matching and not affecting each element amplitude and phase. The design analysis is done to meet following objectives:

a) The in-phase feeding between output ports;

b) The power division in such a way that it does not cause high side lobes;

c) Low insertion feeding loss and good impedance matching.

The design of power divider is done on Rogers 5880 with a relative dielectric permittivity ε_r=2.2 and a loss tangent tan δ = 0.0009 with 0.508 mm (20 mils) thickness for 32.5 GHz solution frequency. The diameter of via is 0.5 mm with spacing between two vias as 0.9 mm. The current distribution for this power divider is illustrated in Fig 4.2, which depicts the unequal power flow in series feeding network.

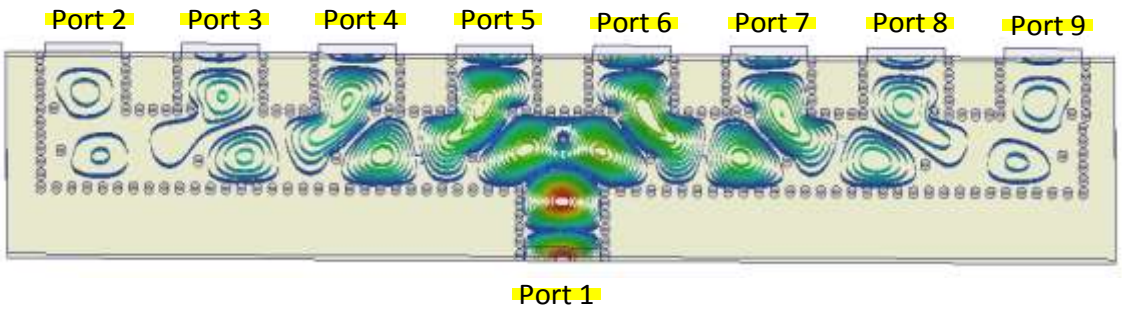

Fig. 4.2 Current distributions of unequal power division for 1 × 8 SIW series feeding divider.

The return loss for the input port and each output port is shown in Fig. 4.3. It is observed that there is good impedance matching as S_{11} is below -15 dB over the whole frequency range of 29-36 GHz. The return loss at output ports depicts that this feeding network has insertion losses as feeding network is not designed to provide a balanced power division over a wide band and losses are bit obvious due to amplitude balance of the divider. Moreover with the insertion loss compensation of ~1 dB, the benefits of high gain and low side lobe levels are still achievable.

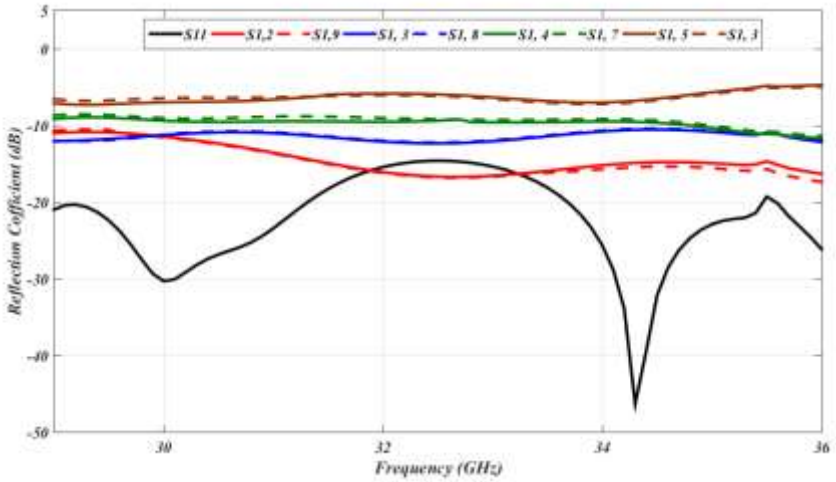

Fig. 4.3 Reflection coefficient (S-parameters) of all ports (Input port (S_{11}) and output ports (S_{12} – S_{19}).

The phase at each output port is equally important to have good impedance matching at desired solution frequency of 32.5 GHz. Fig 4.4 illustrates in phase at each output port. It is seen that the phase at ports 2-5 is same at ~ -90° and ports 6-9 meet around the same angle ~ 90°. The in-phase matches at frequency 32.5 GHz and with a tolerance level of ±1 GHz, as a consequence this design can be considered for its neighboring frequencies also.

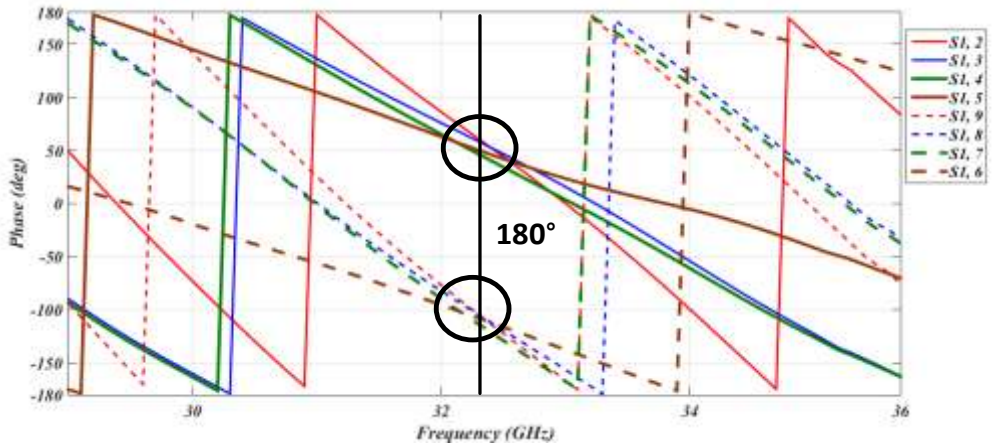

Fig. 4.4 Phase (deg) distribution at each output port with respect to input port

4.3 Proposed Antipodal Fermi Linear Tapered Slot Antenna Array

The antipodal fermi linear tapered slot antenna, which is analyzed in chapter 3, is used to construct an array antenna using 1 × 8 SIW series feeding divider as shown in Fig. 4.5 (a). The tapered slot antenna on either side of Rogers 5880 is shown in Fig. 4.5 (b, c). This planar AFLTSA array is simulated using Ansys HFSS and CST Microwave studio. The overall size of this array structure is 64 mm × 88 mm × 0.508 mm. The design parameters are tabulated in Table 4.1 along with the specifications of adaptive vias (C1-C5) with respect to the origin as illustrated in Fig. 4.1

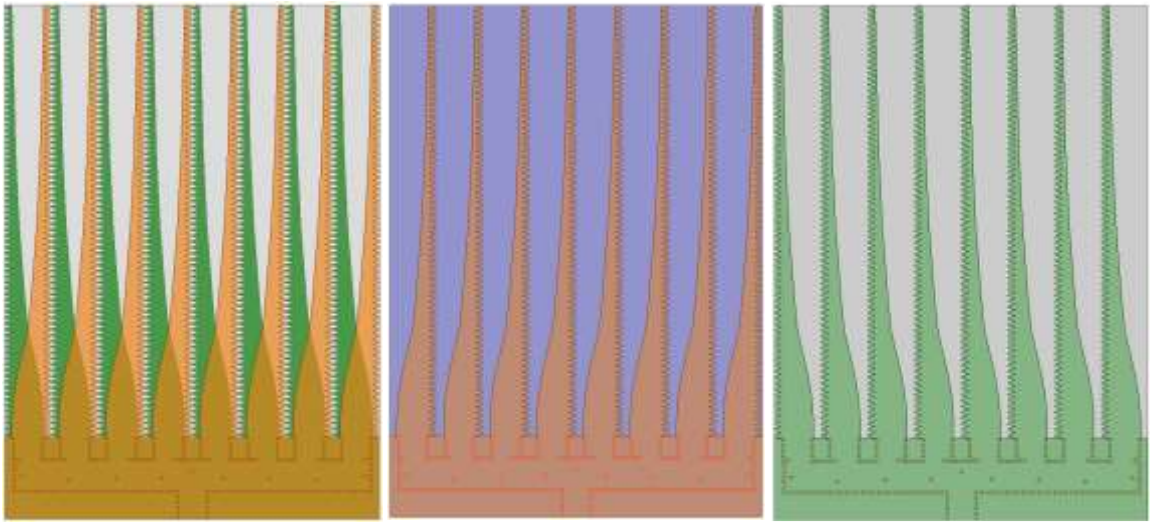

Fig. 4.5 (a) 1 × 8 SIW based AFLTSA array (b) Top view of array structure (c) Bottom view of array structure.

Table 4.1: Optimized parameters of the AFLTSA array using SIW power divider

Parameter	**wsiw**	**pd_l**	**pd_w**	**ms_w**	**ms_l**	**d**	**s**
Value (mm)	5	14	64	1.61	5	0.5	0.9
Parameter	**C1**	**C2**	**C3**	**C4**	**C5**		
Value (mm)	(30.5, 3.44)	(30.5, 3.44)	(30.5, 3.44)	(30.5, 3.44)	(30.5, 3.44)		

4.4 Results and Discussions

The simulated results of this proposed array structure is presented in this section and the fabrication is underway and will be acknowledged in the future.

4.4.1 Return Loss Calculations

The 1 × 8 SIW based AFLTSA array is simulated in HFSS and CST and calculated results are discussed in this section. The fabrication is due in the future due to time constraints,

but the simulation done in both software ensures that the desired measured results will be near to the calculated results.

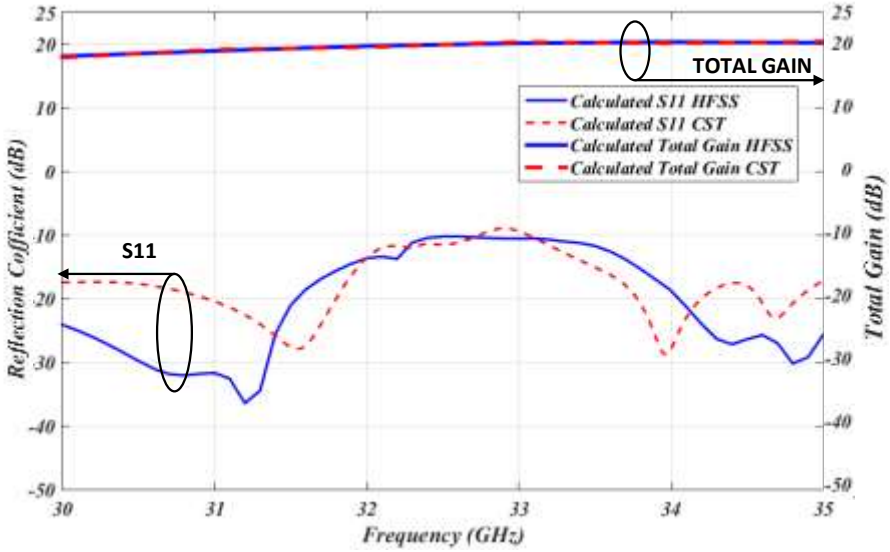

Fig. 4.6 Return loss over impedance bandwidth and total gain achieved in HFSS and CST.

The return loss calculations, as shown in Fig. 4.6 shows a wide impedance bandwidth (S_{11} < -10 dB) between 30-35 GHz, which accounts for 14.7 % of the solution frequency. It is normal that the bandwidth decreases with the increase in the number of elements in an array form, but this array structure has attained an acceptable bandwidth over the desired frequency range. The gain achieved is 18.1-20.4 dB over the impedance bandwidth, which results in very high gain antenna structure. The results have taken into account the insertion losses from SIW power divider and also have taken copper as top and bottom layer instead of PEC. The losses account to 1.2 dB as the single element AFLTSA's gain is 12.6 dB, whereas the array gain obtained at 32.5 GHz is 20.4 dB.

4.4.2 Radiation Pattern Characteristics

Apart from obtaining wide impedance bandwidth for an array AFLTSA, it is important to analyze its radiation pattern characteristics which include the calculated gain and the side lobe levels in both the planes: E-plane and H-plane. The total gain achieved at 32.5 GHz using both the simulation tools is shown in Fig. 4.7.

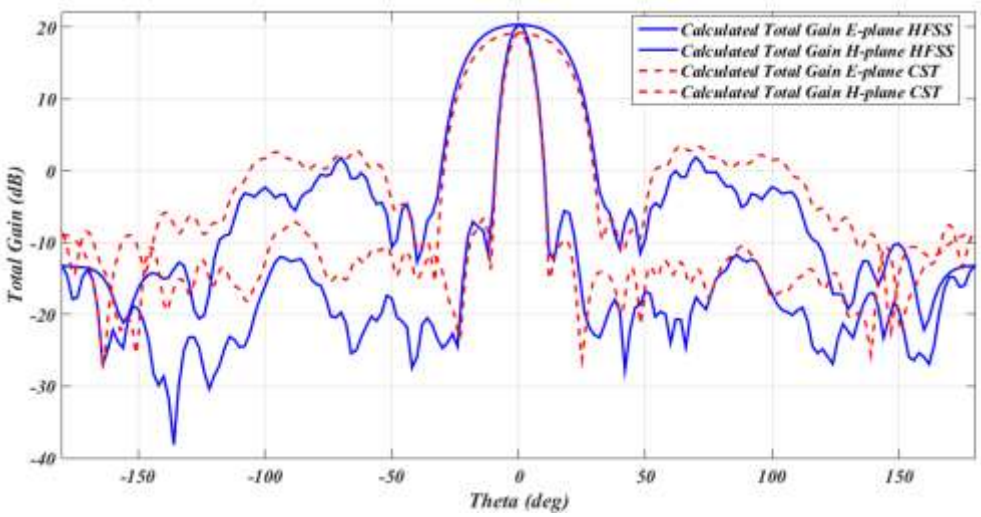

Fig. 4.7 Total gain calculated in HFSS and CST for 1 × 8 AFLTSA array

It is observed that the gain of 20.4 dB is obtained with SLL better than 25.97 dB and 18.5 dB in E-plane and H-plane respectively using HFSS simulating tool. Whereas in CST, SLL is better than 25.98 dB and 15.7 dB in E-plane and H-plane respectively. Therefore, the sidelobe levels calculated are less than -25 dB in E-plane and -15 dB in H-plane, which accounts for an objective of designing SIW series feeding power divider. The calculated radiation efficiency over the wide impedance bandwidth ranges between 90% - 91%. The maximum radiation efficiency occurs at 32.5 GHz, which is the solution frequency. However, it is evident that with an increase in gain, the beam becomes narrower; therefore,

the 3dB beamwidth calculated is 8.35° and 35.16° in E-plane and H-plane respectively. The calculated final results are tabulated in Table 4.2.

Table 4.2: Total Gain and side lobe level characteristics of 1 × 8 AFLTSA array

Simulation tool	Total Gain	SLL (E-plane)	SLL (H-plane)	3 dB Beamwidth
HFSS	20.4 dB	Better than 25.9 dB	Better than 18.5 dB	8.35° (E) - 35.16° (H)
CST	19.8 dB	Better than 25.9 dB	Better than 15.7 dB	8.3° (E) – 34.9° (H)

Similarly, the radiation pattern is calculated over the impedance bandwidth as shown in Fig. 4.8 with their respective gains and 3 dB beamwidth as tabulated in Table 4.3. These results show a promising nature of this antenna array for obtaining measured gain over the wide impedance bandwidth.

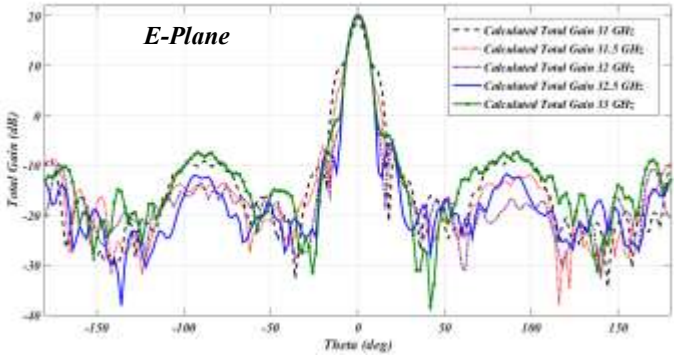

(a)

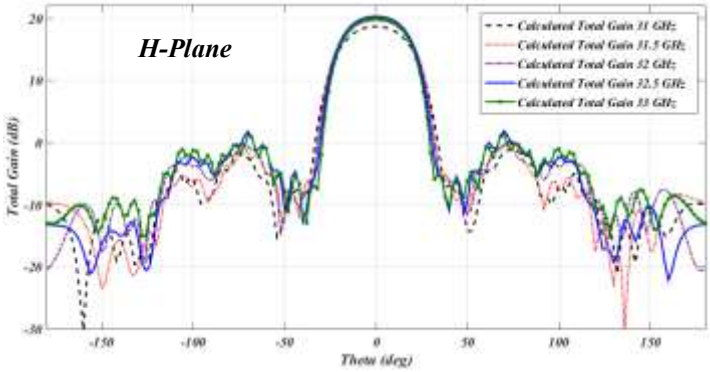

(b)

Fig. 4.8 (a) E-plane calculated pattern results for 31-33 GHz. (b) H-plane calculated pattern results for 31-33 GHz.

Table 4.3: Performance radiation characteristics of 1 × 8 AFLTSA array

F (GHz)	Total Gain	SLL (E-plane)	SLL (H-plane)	3 dB Beamwidth	Efficiency
31	18.7 dB	< -27.3 dB	< -19.69 dB	8.31° (E) – 36.6° (H)	90.1 %
31.5	19.6 dB	< -25.27 dB	< -19.46 dB	8.25° (E) – 37.16° (H)	90.35 %
32	19.8 dB	< -25.49 dB	< -19.52 dB	8.24° (E) - 35.8° (H)	91.2 %
32.5	20.4 dB	< -25.97 dB	< -18.52 dB	8.35° (E) – 34.16° (H)	90.5 %
33	20 dB	< -24.09 dB	< -18.8 dB	8.26° (E) – 33.96 ° (H)	90.5 %

4.5 Summary

In this chapter, a 1 × 8 substrate integrated antipodal fermi linear tapered slot antenna is analyzed. Firstly, a 1 × 8 SIW power divider is discussed, and its return loss and phase distribution are presented. The power divider has unequal power division with adaptive vias that are placed in it to have better impedance matching at different ports. Then, the whole antenna array is simulated using both CST and HFSS simulating tools and a wide bandwidth of 14.7 % is achieved over the frequency range of 30-35 GHz. The gain obtained is also high and ranges between 18.1-20.4 dB for the same frequency range. Apart from the obtained gain, the sidelobe levels in both E- and H- planes, the 3 dB beamwidths, and radiation efficiencies are tabulated in Table 6 and Table 7, which prove this proposed antenna array to be a promising candidate for millimeter wave applications.

Chapter 5: Substrate Integrated Beamforming AFLTSA

5.1 Introduction

After analyzing the performance characteristics of a single element and 1 × 8 array configuration of antipodal fermi linear tapered slot antenna, the next step is to analyze this antenna in a beamforming network. In this chapter, the designing of beamforming networks for 2 × 2 and 4 × 4 subarrays is discussed in section 5.2. The design is done using s-parameters technique, which ensures the accurate design of multimode section of BFN. In section 5.3, a parametric study and performance characteristics of beamforming networks is presented using Ansys HFSS. The proposed design of AFLTSA beamforming subarrays is presented in section 5.4 with their design specifications. After the parametric study analysis, the fabrication process and measurement setup is explained in section 5.5 followed by results and discussions in section 5.6 and summary in section 5.7.

The beamforming networks are designed on substrate Rogers 5880, with a relative dielectric permittivity ε_r=2.2 and a loss tangent tan δ = 0.0009 with 0.508 mm (20 mils) thickness for 32.5 GHz solution frequency.

5.2 Design methodology of beamforming networks

The design of beamforming networks is based on theoretical equations using s-parameters technique [63]. There are some points to be considered before designing beamforming networks.

a) The beamforming network for AFLTSA should be symmetrical because the width of the antenna is more than the SIW width.

b) The beamforming network should comprise of multimode section (no phase shifters) for controlling the phase between each output port.

c) The number of elements are limited as with the increase in elements; it is more difficult to control the phase between each port.

In Fig 5.1 the beamforming networks for 2 × 2 and 4 × 4 subarrays using multimode section technique are presented. Here Moder 1 and Moder 2 represents the fields' amplitude transformation, which can excite different modes within the multimode section while the multimode section is used to achieve and control phase transformation as the amplitude of each mode propagated is invariant with respect to the longitudinal direction.

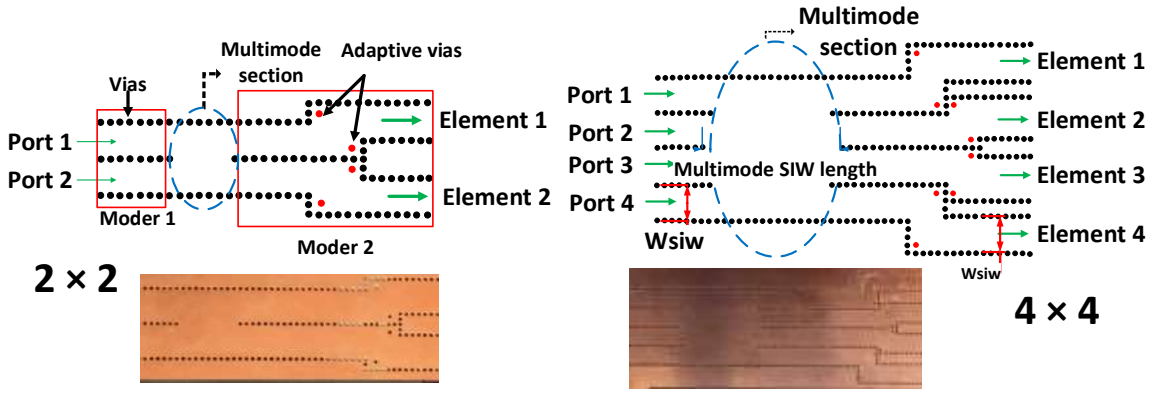

Fig. 5.1 2 × 2 and 4 × 4 beamforming structures using multimode sections

The study of calculating multimode section length can be analyzed using s-parameters [63] and we will be analyzing these lengths for 2 × 2 and 4 × 4 sub arrays structures as shown in Fig.5.1.

Let us denote moder 1 and moder 2 as $[M_1]$ and $[M_2]$, respectively. These two matrices should be symmetrical therefore, $[M_1] = [M_2]^T$ and consider this symmetrical BNF as lossless. There is a relation between input ports and number of modes in this section ($N = 2^n$, where n is 1, 2, 3….). If we consider [S] as an N x N sub matrix of $[M_1]$ and $[M_2]$, and [X] is a submatrix of [Y], we can express them as equation 5.1 and 5.2 and considering the multimode SIW length as x_o, following relations can be developed.

$$[M_2]^T = [M_1] = \begin{bmatrix} [0] & [S] \\ [S]^T & [0] \end{bmatrix} \tag{5.1}$$

$$[Y] = \begin{bmatrix} [0] & [X] \\ [X] & [0] \end{bmatrix} \tag{5.2}$$

Matrix X can be expressed as:

$$x_{ij} = \delta_{ij} e^{j\beta_n x_o} \tag{5.3}$$

where, δ_{ij} is Kronecker delta and β_n is propagation constant corresponding to different nodes.

Using equations 5.1, 5.2 and 5.3 we can write total s-parameters as:

$$[S_{TOTAL}] = \begin{bmatrix} [0] & [S][X][S]^T \\ [S][X][S]^T & [0] \end{bmatrix} \tag{5.4}$$

For $[S_{TOTAL}]$ to be S-matrix for BNF it should satisfy:

$$[D][0] = \big[[0][F]\big][S_{TOTAL}] \tag{5.5}$$

where, [D] is symmetrical and unitary matrix of order N and its rows represents the aperture illumination for an excitation, [F] is an identical matrix whose rows are for input ports for excitation with unit amplitude.

And finally with a help of equation 5.6 and 5.7, we can calculate the multimode SIW length with respect to error in phase between moder 1 and moder 2.

$$\beta_n x_o - b_n = 2m\pi \qquad n = 1,2,\ldots.N \tag{5.6}$$

$$d_{pq} = \frac{1}{\sqrt{N}} e^{-\left(\frac{j\pi}{N}\right)[(2p-1)-q]} \tag{5.7}$$

Where β is propagation constant for N orthogonal uniform beams and d_{pq} can be expressed for[D]. Therefore, the length of SIW multimode section can be determined for 2 × 2 sub-array as:

$$\mathbf{x_o} = \frac{\boldsymbol{\pi}}{\mathbf{2(\beta_1 - \beta_2)}} \tag{5.8}$$

Similarly, the multimode section length for 4 × 4 sub arrays can be determined between each port but needs more optimization to reduce the phase error. The theoretical phase error vs the multimode section length with respect to the excitation from different ports can be illustrated in Fig. 5.2. It is observed that for 2 × 2 subarray structure, there is a phase control when multimode section length is approximately 9.6 mm, whereas this length ranges between 18-20 mm for 4 × 4 subarray structure.

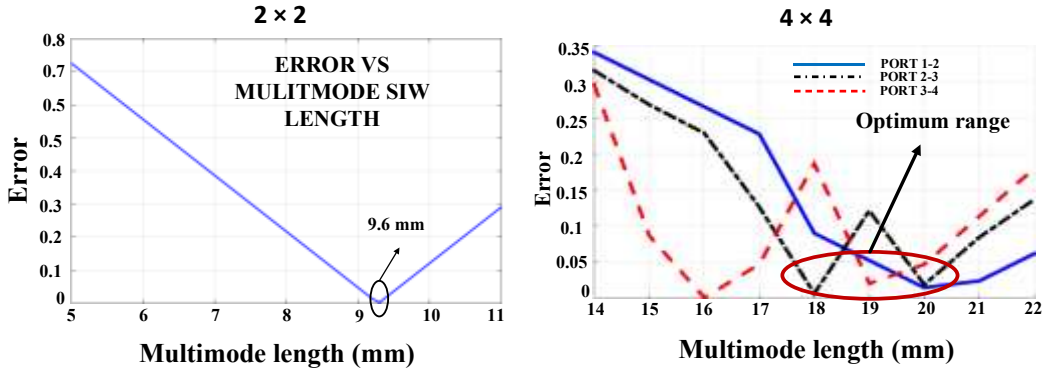

Fig. 5.2 Phase error diagram with multimode section length (mm) for 2 × 2 and 4 × 4 sub-array structures

5.3 Parametric Analysis

5.3.1 2 × 2 subarray beamforming network

A parametric study for 2 × 2 subarray structures is conducted with respect to different multimode section lengths. In Fig 5.3, the reflection coefficient (S_{11}) and the phase between output ports of multimode section lengths 7mm, 9.6mm, 11mm are analyzed. The best value (9.6mm) gives reflection coefficient below -20 dB with a phase difference between output ports of 90°.

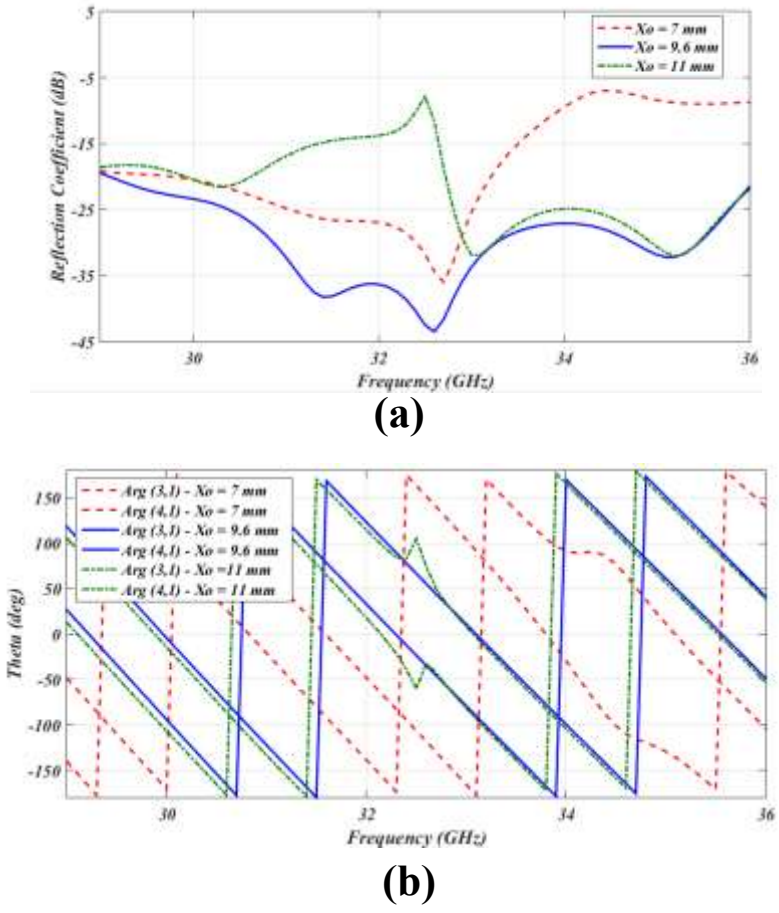

Fig. 5.3 (a) Reflection coefficient magnitude and (b) Phase difference between output ports for x_o = 7mm, 9.6mm and 11 mm

The phase difference between output ports at 32.5 GHz is 81°, 90° and 104° for multimode section lengths of 7mm, 9.6mm, and 11mm respectively. Therefore, this length is very sensitive to perform beamforming action and should be analyzed carefully. The current distribution for $x_o = 9.6$mm is shown in Fig 5.4, which illustrates the current flow from port 1 to both the output ports.

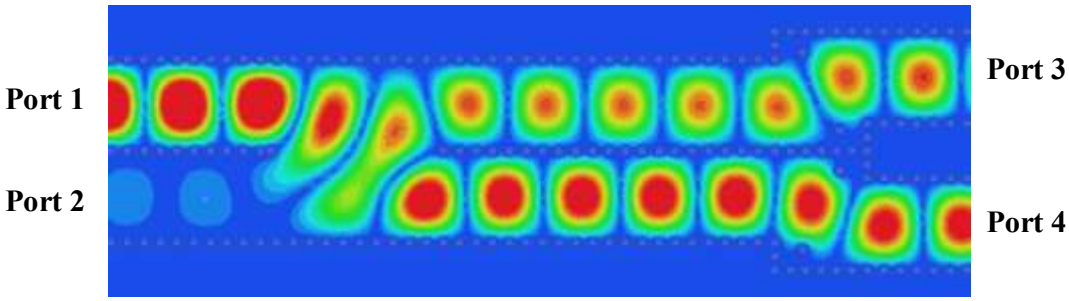

Fig. 5.4 Current distribution - 32.5 GHz for 2 × 2 sub-array structure excited from port 1.

The final s-parameters calculations are presented in Fig. 5.5 with return loss at all ports when excited from port 1. It must be noted that we obtained similar results either excited from port 1 or port 2 as there are only two input ports.

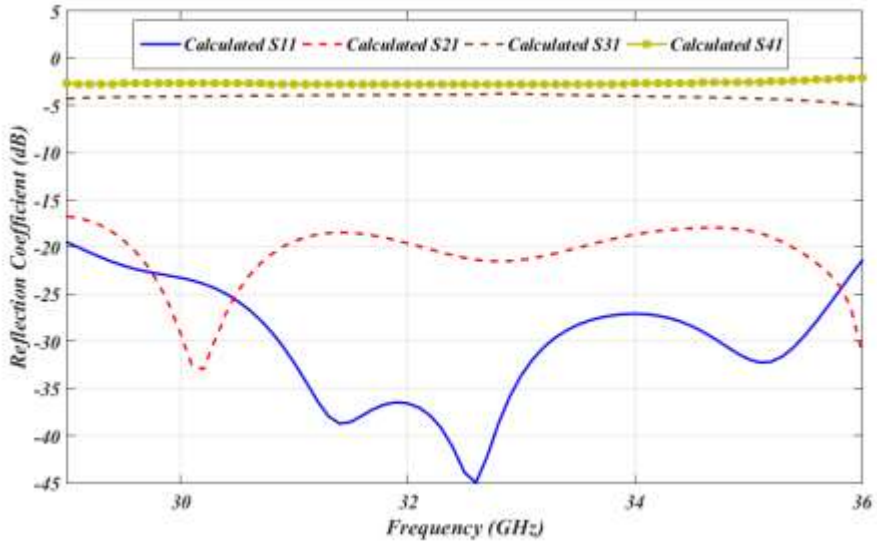

Fig. 5.5 Reflection coefficient for 2 × 2 sub-array structure excited from port 1

5.3.2 4 × 4 subarray beamforming network

A parametric study for 4 × 4 subarray structures is divided into two parts: firstly, with multimode section length equal to 18 mm and secondly, with the length of 19.8 mm. The purpose of dividing the parametric analysis into two parts is to analyze return loss when either excited from port 1 or port 4 and excited from port 2 or port 3 for two different lengths. Note that the multimode section lengths range between 18-20 mm.

X_o = 18 mm

The reflection coefficient magnitudes when excited from port 1 and port 2 are presented in Fig. 5.6 (a) and 5.6 (b). As the number of elements increase, it is difficult to control the matching and phase difference between the ports. It is observed that there is a lot of fluctuations in the return loss which is below -10 dB for the solution frequency of 32.5 GHz. Also, there is a good coupling with the other ports, which are connected to 50 ohm loads.

X_o = 19.8 mm

Similarly, the s-parameters for multimode section length as 19.8 mm is calculated when excited from port 1 and port 2. The reflection coefficient when excited from port 1 and port 2 are presented in Fig. 5.6 (c) and 5.6 (d). It is observed that at this length, the fluctuations are less and have better return loss than at 18 mm. Therefore, this analyzed length will be used as design specifications.

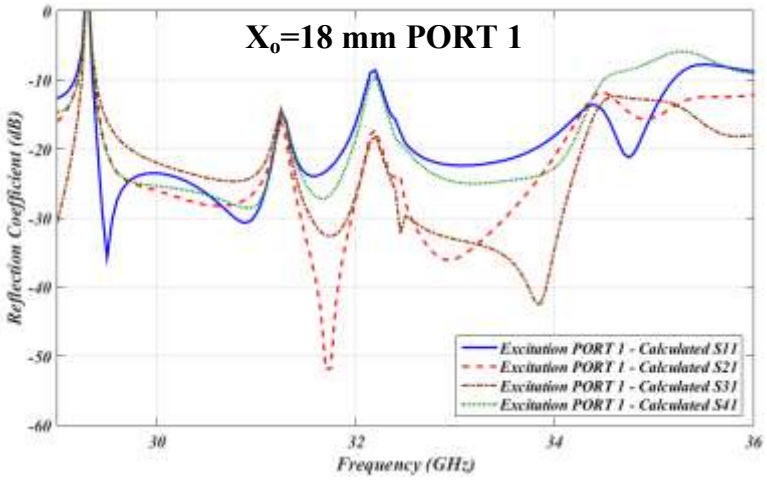
X₀=18 mm PORT 1
Reflection Coefficient (dB)
Frequency (GHz)
Excitation PORT 1 - Calculated S11
Excitation PORT 1 - Calculated S21
Excitation PORT 1 - Calculated S31
Excitation PORT 1 - Calculated S41

(a)

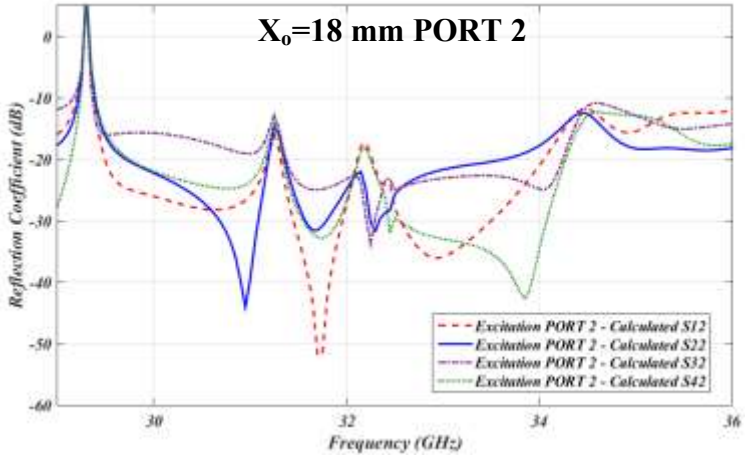
X₀=18 mm PORT 2
Reflection Coefficient (dB)
Frequency (GHz)
Excitation PORT 2 - Calculated S12
Excitation PORT 2 - Calculated S22
Excitation PORT 2 - Calculated S32
Excitation PORT 2 - Calculated S42

(b)

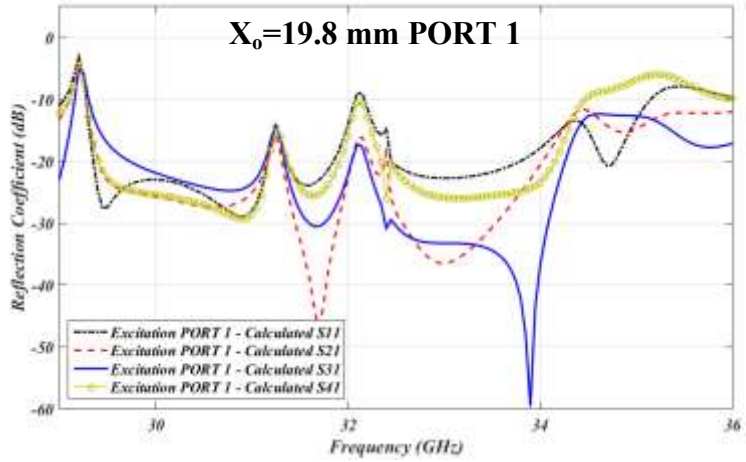
X₀=19.8 mm PORT 1
Reflection Coefficient (dB)
Frequency (GHz)
Excitation PORT 1 - Calculated S11
Excitation PORT 1 - Calculated S21
Excitation PORT 1 - Calculated S31
Excitation PORT 1 - Calculated S41

(c)

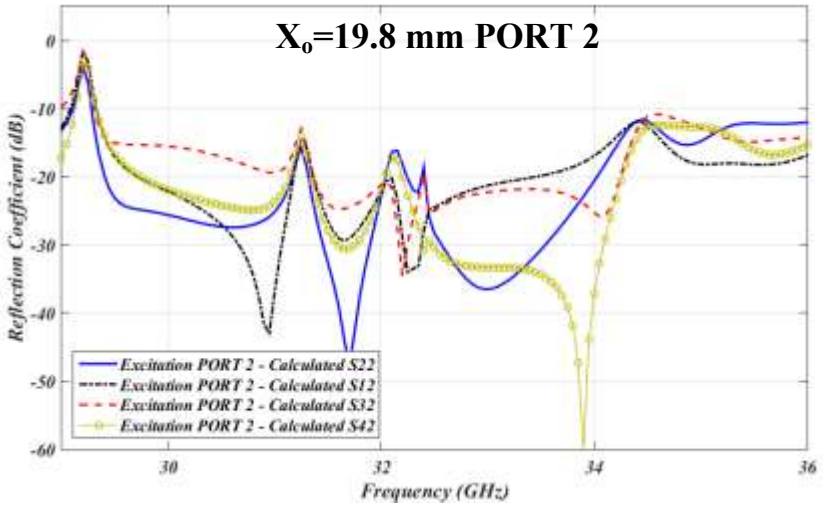

(d)

Fig. 5.6 Reflection coefficient for 4× 4 subarray structure (a) with x_o = 18 mm excited from port 1 (b) with x_o = 18 mm excited from port 2 (c) with x_o = 19.8 mm excited from port 1 (d) with x_o = 19.8 mm excited from port 2

The current distributions for this length are presented in Fig 5.7 when excited from port 1 and port 2. This current distribution depicts the rotation of beam, which is the main concept of beamforming using beamforming networks. It is also clearly seen as the multimode length increase with an increase in the number of elements, it is more difficult to control the phase within the multimode section.

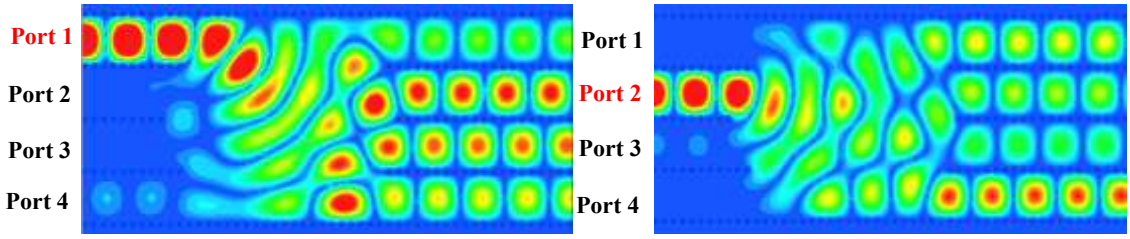

Fig. 5.7 Current distribution -32.5 GHz for 4 × 4 subarray structure excited from port 1-2.

5.4 Fabrication and Measurement setup

This section deals with the fabrication process and measurement setup required for such beamforming antennas. There are various steps which should be considered before proceeding with the fabrication process for beamforming networks.

5.4.1 Microstrip-SIW transition

There has to be a microstrip-SIW transition for each port in above 2 × 2 and 4 × 4 sub arrays in order to connect the suitable connectors for exciting the antenna through microstrip. Therefore, a new configuration is adapted without affecting the results. This configuration, as shown in Fig 5.8 for both the subarrays, help not only in the feasible configuration for connecting connectors but also help in reducing side lobe levels, which will occur while performing beamforming operation.

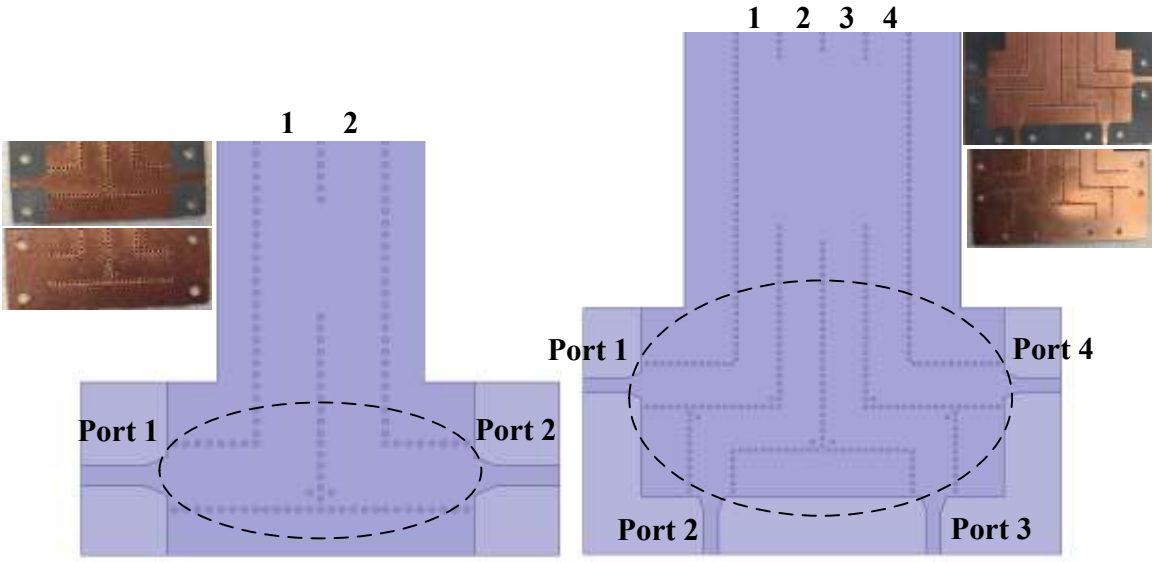

Fig. 5.8 Microstrip-SIW new configuration for fabrication process

This increases the size of overall structure but help in easy fabrication process and reducing side lobe levels.

5.4.2 Choice of connectors and 50 Ω loads

Return loss measurement is performed using Agilent PNA N5227A (67 GHz) network analyzer. But before performing return loss measurement, the choice of connectors and loads is important. The connector that is used for this proposed antenna is Southwest Microwave 2.92mm Jack (female) end launch connector [64], which has metal screws to hold the antenna structure. There is one problem, which is encountered during the measurement process: the width of the microstrip line is more than the dielectric diameter of the connector, which could make the whole circuit as a short circuit. Therefore, it is necessary to taper the microstrip line in order to avoid short circuit or else, we can use the testing fixture, which is limited to 2 port antenna. There is a technique as explained in one of the technical documents of Southwest Microwave, which illustrates the phenomenon of tapering of the microstrip line with minimum effect on impedance matching. This technique is illustrated in Fig 5.9 [65]. It is shown in Fig. 5.9 (c), the optimized taper version for this connector can be used which has minimum effect on impedance matching and is an effective way to overcome our problem. For instance, the optimized tapered version can be seen in Fig. 5.10 (c) from 4 × 4 subarray antenna. The 50 Ω load used for millimeter wave band is SigaTek LMS-2 (2.4mm male), and it can be connected to the connector with a help of an adapter. The connector and 50 Ω load are illustrated in Fig 5.10

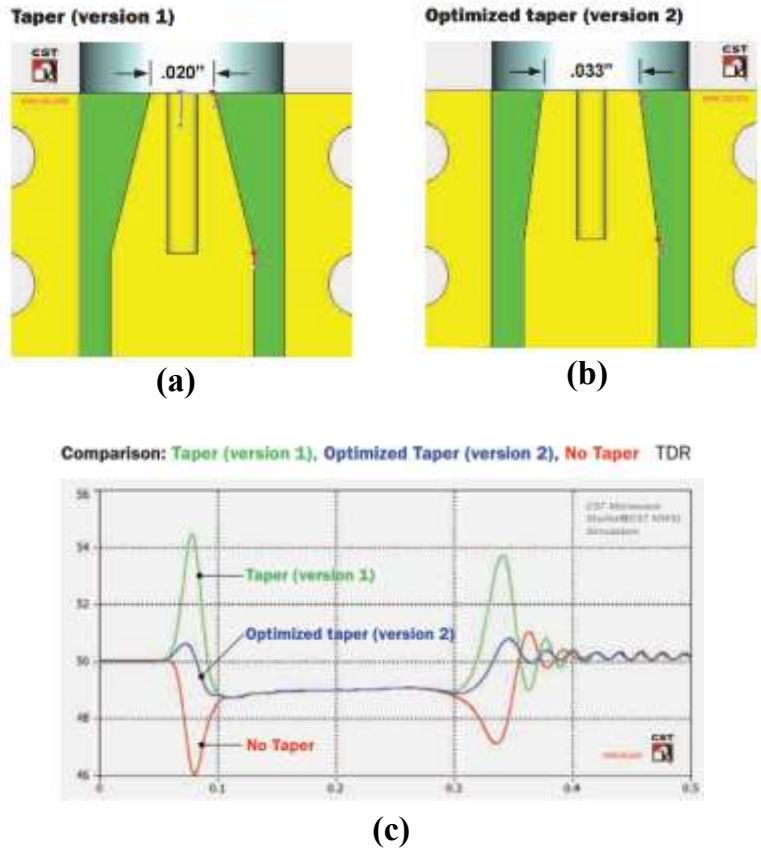

Fig. 5.9 Determination of optimal launch (a) Taper version 1 (b) Optimized taper version 2 (c) Impedance graph for all taper versions [65]

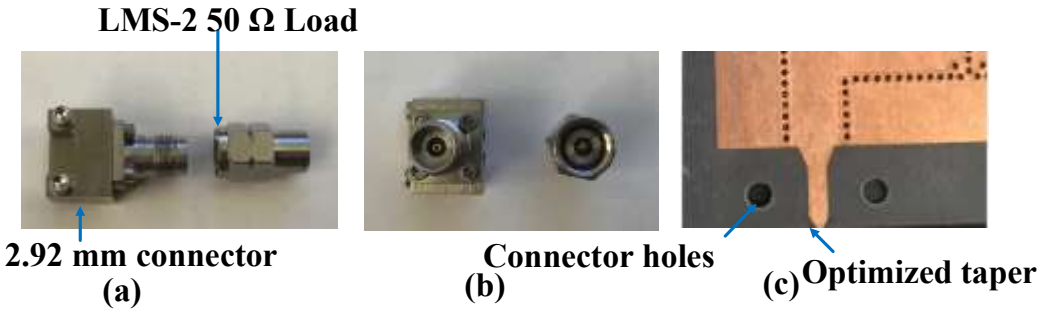

Fig. 5.10 (a) End launch 2.92 mm connector and LMS-2 50 Ω load. (b) Top view of connector and load (c) Fabricated tapered version

5.4.3 Mounting structures

The mounting structures are also fabricated for each antenna structure in order to measure the radiation pattern in the anechoic chamber. As this is a multibeam antenna, special holding structures are fabricated. We use ABS (plastic) material for fabricating these mounting structures and absorbers are put over it to reduce the impact of plastic on antenna structure. Fig 5.11 shows the fabricated designs and models made in SolidWorks software for 2 × 2 and 4 × 4 sub arrays. The design is made keeping in mind the antenna size, weights of connectors, loads, and cables.

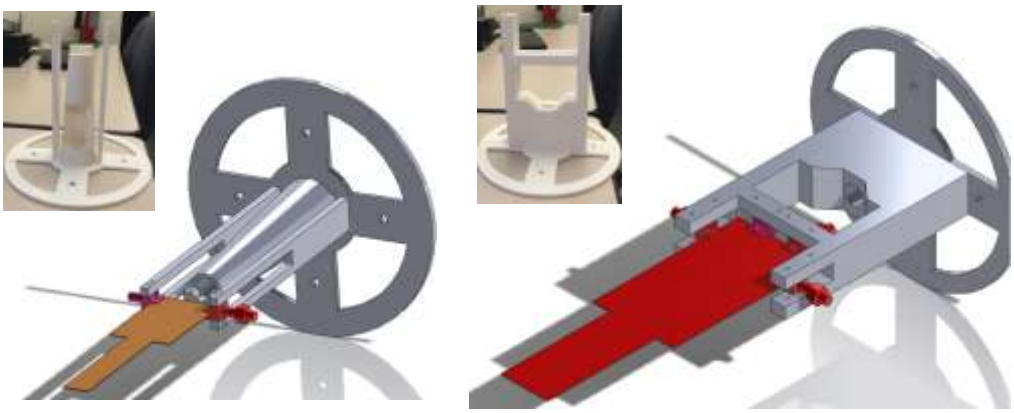

(a) **(b)**

Fig. 5.11 Mounting structure for (a) 2 × 2 subarrays (b) 4 × 4 subarrays.

5.5 Result and Discussions

5.5.1 2 × 2 Antipodal Fermi Linear Tapered Slot Antenna Subarray

The antenna is simulated in Ansys HFSS. The simulation and measurement results of the proposed structure are compared and discussed in this section. There is a very good agreement between the measured and simulated results at millimeter wave frequency band.

The fabricated antenna is presented in Fig 5.12, which is initially analyzed by testing fixture and then by connectors.

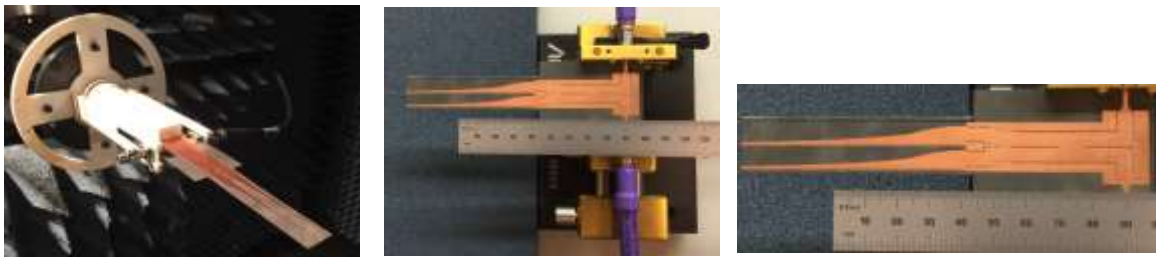

With Connectors **With Testing Fixture** **2 × 2 AFLTSA**

Fig. 5.12 Fabricated 2 × 2 AFLTSA structure with connectors and testing fixture.

The proposed structure is measured using testing fixture and using connectors (each port is excited at one time) for measuring the reflection coefficient. It is seen in Fig. 5.13 (a) that the results with testing fixture are more accurate than using connectors because of tapering the microstrip width, there will be a little bit change in impedance matching. The measured reflection coefficient is below -10 dB over the frequency range 29-36 GHz obtaining 21.54 % impedance bandwidth. The radiation performance characteristics are illustrated in Fig 5.13 where the beam is rotated only in E-plane at ± 6° with excitation from either port. It is observed that in order to satisfy the Fermi-Dirac equation in equation 3.11, the length of the antenna is too long for beam rotation.

The total gain measured at 32.5 GHz is 12.2 dB with 19.2° 3 dB beamwidth, when excited from port 1 and is 12.029 dB with 20.5° 3 dB beamwidth, when excited from port 2 in comparison to single element gain of 12.6 dB.

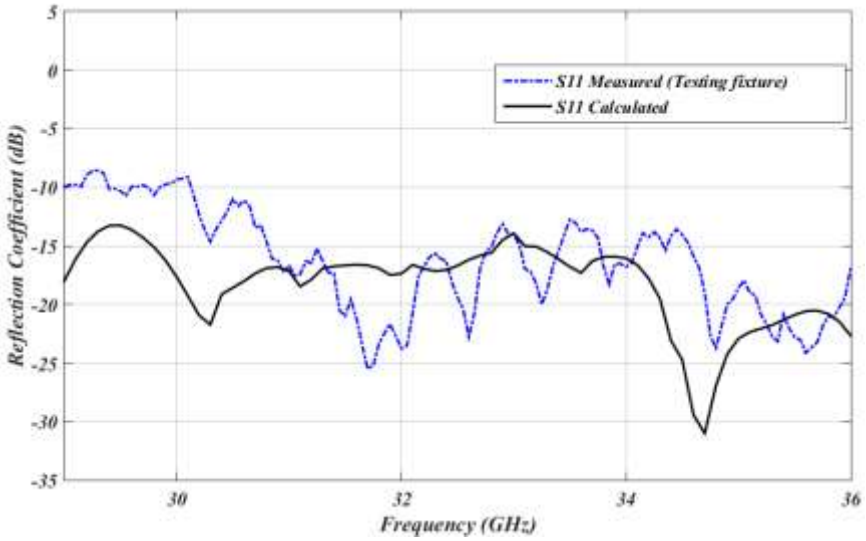

(a)

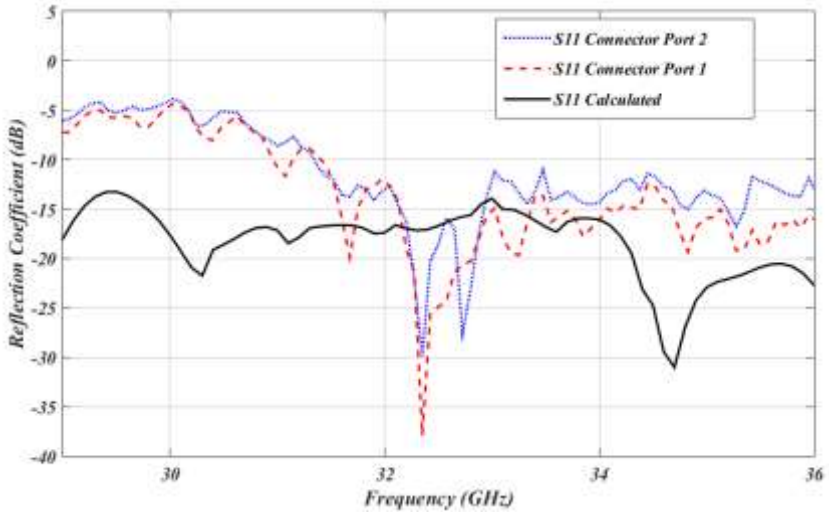

(b)

Fig. 5.12 Reflection Coefficient (S_{11}) with use of (a) testing fixture and (b) connectors.

The normalized gain in E-plane with calculated and measured results are shown in 5.13 in polar and rectangular form.

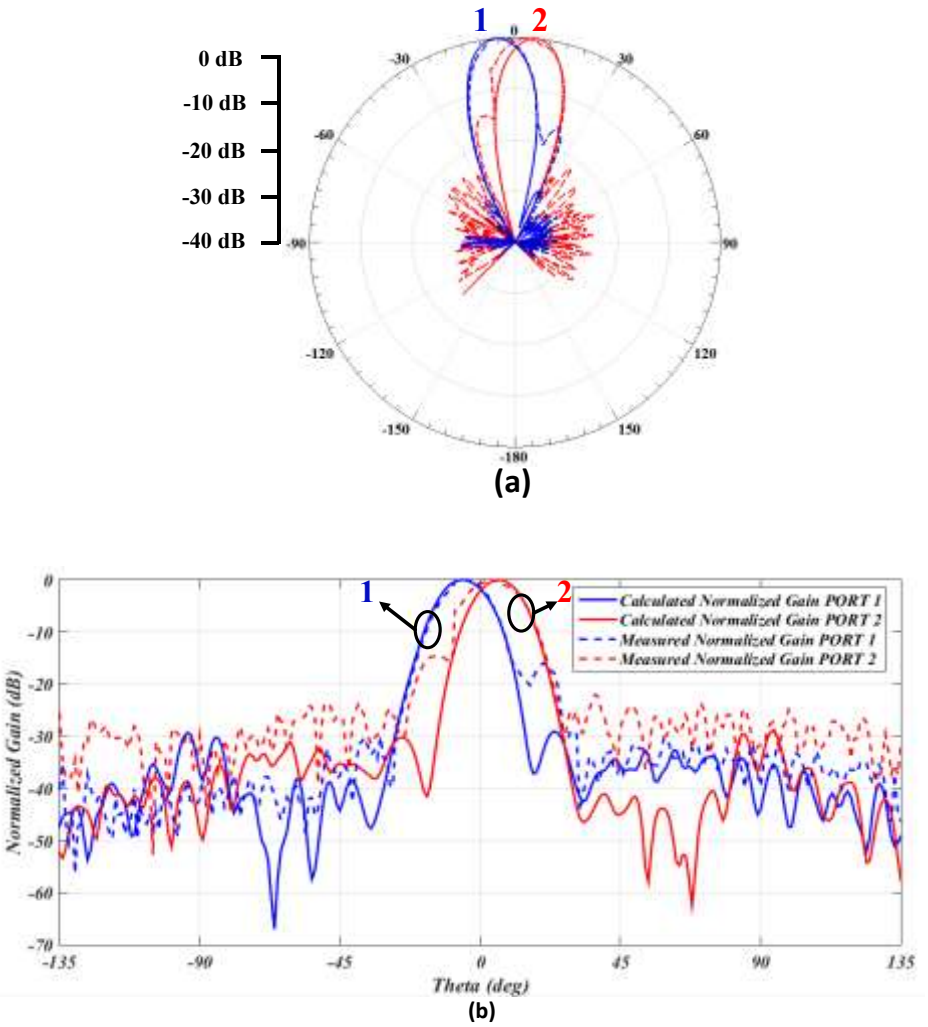

Fig. 5.13 Calculated and measured normalized gain in (a) polar form (b) rectangular form.

It is clearly shown that the measured side lobe level is better than -17.2 dB from port 1 and -14.8 dB from port 2. The minor lobes are much higher than the simulated results because of the atmospheric conditions and practical considerations of the anechoic chamber. There are always high side lobes when the beam is rotated in multibeam antenna, but the analyzed phase control and microstrip-SIW transition structure helps in reducing side lobe levels. The calculated and measured total gain along with beam rotation and 3 dB beamwidth is tabulated in Table 5.1 and is illustrated in Fig. 5.14 (a). Moreover, this subarray structure

has a radiation efficiency of 90.75 % at 32.5 GHz and of 89.96% - 90.97% over the frequency range of 29-36 GHz.

Table5.1: Calculated and measured performance characteristics of 2 × 2 AFLTSA subarray

F (GHz)	Total Gain (dB)			3 dB Beamwidth			Efficiency
	Calculated	Measured (P1/P2)		Calculated	Measured (P1/P2)		
30	10.86	10.52	10.55	21.45°	21.1°	21.9°	90.6 %
30.5	10.77	10.24	10.29	20.81°	20.54 °	21.76°	90.54 %
31	11.44	11.21	11.15	20.79°	20.51°	21.42°	90.64 %
31.5	11.84	11.52	11.53	20.63°	20.35°	21.15°	90.54 %
32	12.1	11.79	11.93	20.11°	19.8°	20.55°	89.96 %
32.5	12.39	12.2	12.029	19.93°	19.2°	20.5°	90.75 %
33	12.05	11.81	11.6	19.5°	18.7 °	20.1°	90.23 %
33.5	11.44	11.18	11.09	18.98°	18.6°	19.5°	90.48 %
34	11.55	11.22	11.13	19.13°	18.8°	19.7°	90.88 %

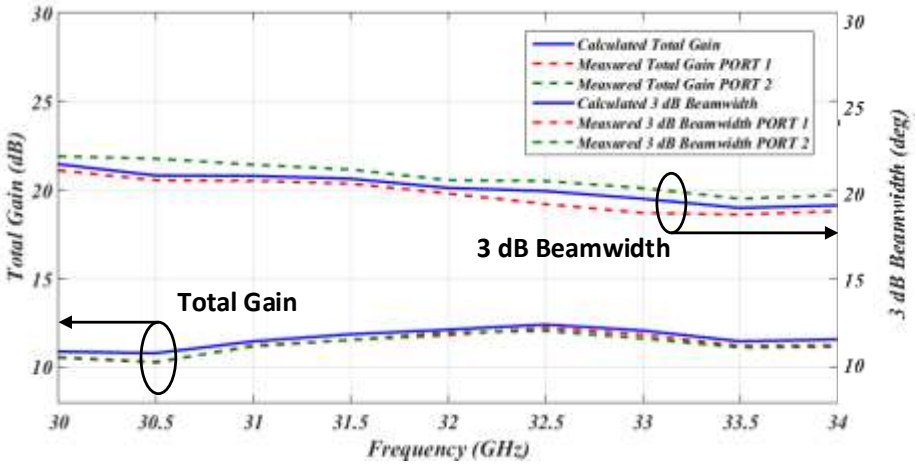

Fig. 5.14 Calculated and measured total gain, and 3 dB beamwidth

5.5.2 4 × 4 Antipodal Fermi Linear Tapered Slot Antenna Subarray

Similarly, 4 × 4 AFLTSA subarray structure is analyzed and simulated in Ansys HFSS to scan the beam in desired directions. It is more complex and difficult to control phase transformation with the increase in elements. In this section, the simulated and measured results are discussed, which indicates the feasibility of this antenna for millimeter wave applications. The fabricated antenna and its mounting in the anechoic chamber are presented in Fig 5.15.

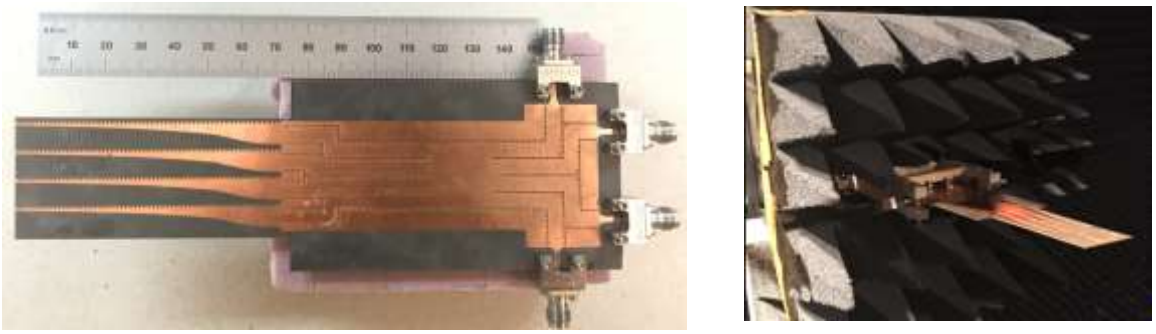

(a) **(b)**

Fig. 5.15 (a) Fabricated 4 × 4 AFLTSA (b) Fabricated 4 × 4 AFLTSA mounted in anechoic chamber.

The proposed structure is an extension of 2 × 2 AFLTSA subarray in order to increase the beam scan angle and the total gain of the antenna. The calculated and measured return loss when excited from port 1 and port 2 is below -10 dB and exhibits a wide impedance bandwidth (31-36 GHz) as shown in Fig 5.16. Due to impedance mismatch (microstrip width tapering), there is a bandwidth reduction with respect to calculated results.

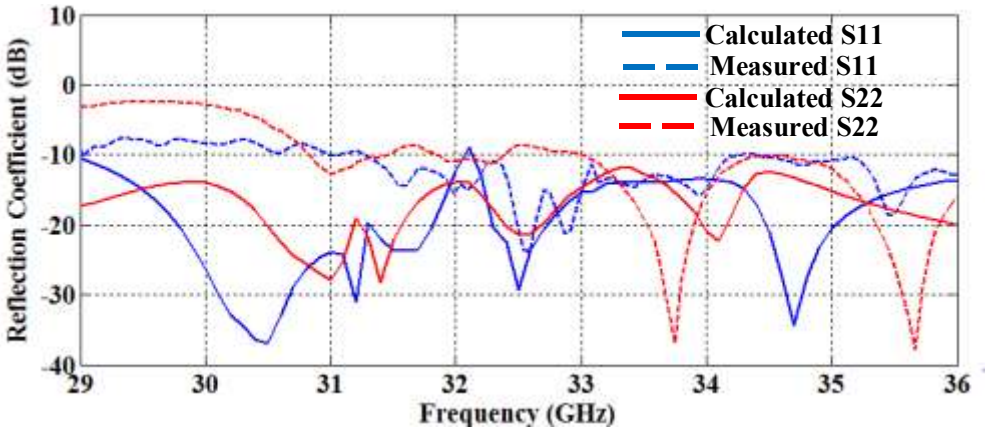

Fig. 5.16 Calculated and Measured S-parameters from port 1 and port 2.

However, there is a good mutual coupling between the excited port and other input ports. The coupling is below -20 dB when excited from any port as shown in Fig 5.17. This mutual coupling is achieved by proper designing of the multimode section and microstrip to SIW transition region.

There are around 1 dB radiation losses which are due to the connectors, practical measurements conditions and use of adapters. The calculated and measured gain in E-plane is shown in 5.18 in rectangular form when excited from each port.

It is clearly understood that there will be high side lobes when the beam is rotated more and consequently the gain decreases (within 3 dB limit). The calculated and measured total gain results are tabulated in Table 5.2.

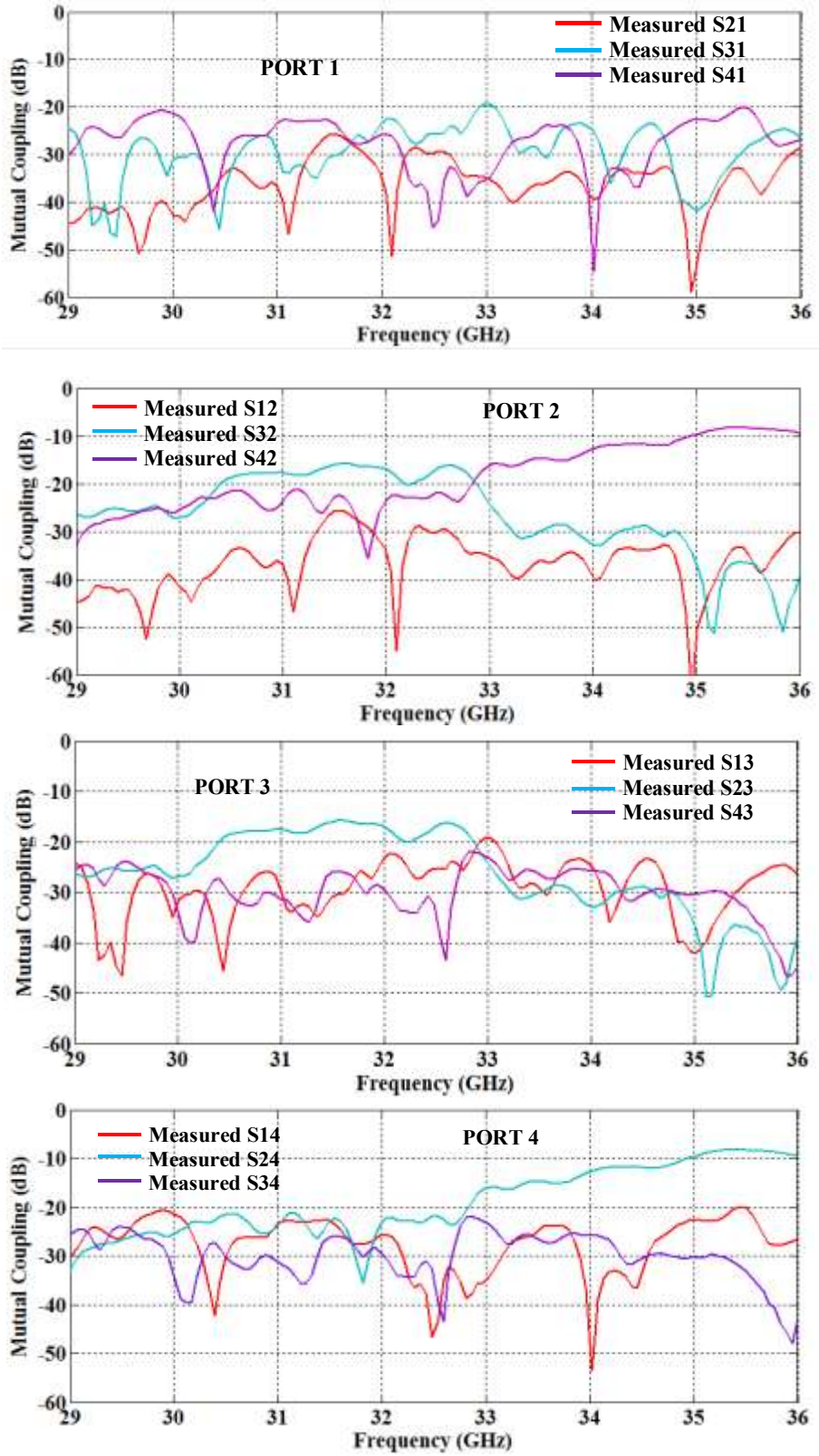

Fig. 5.17 Mutual coupling between the excited port and other input ports.

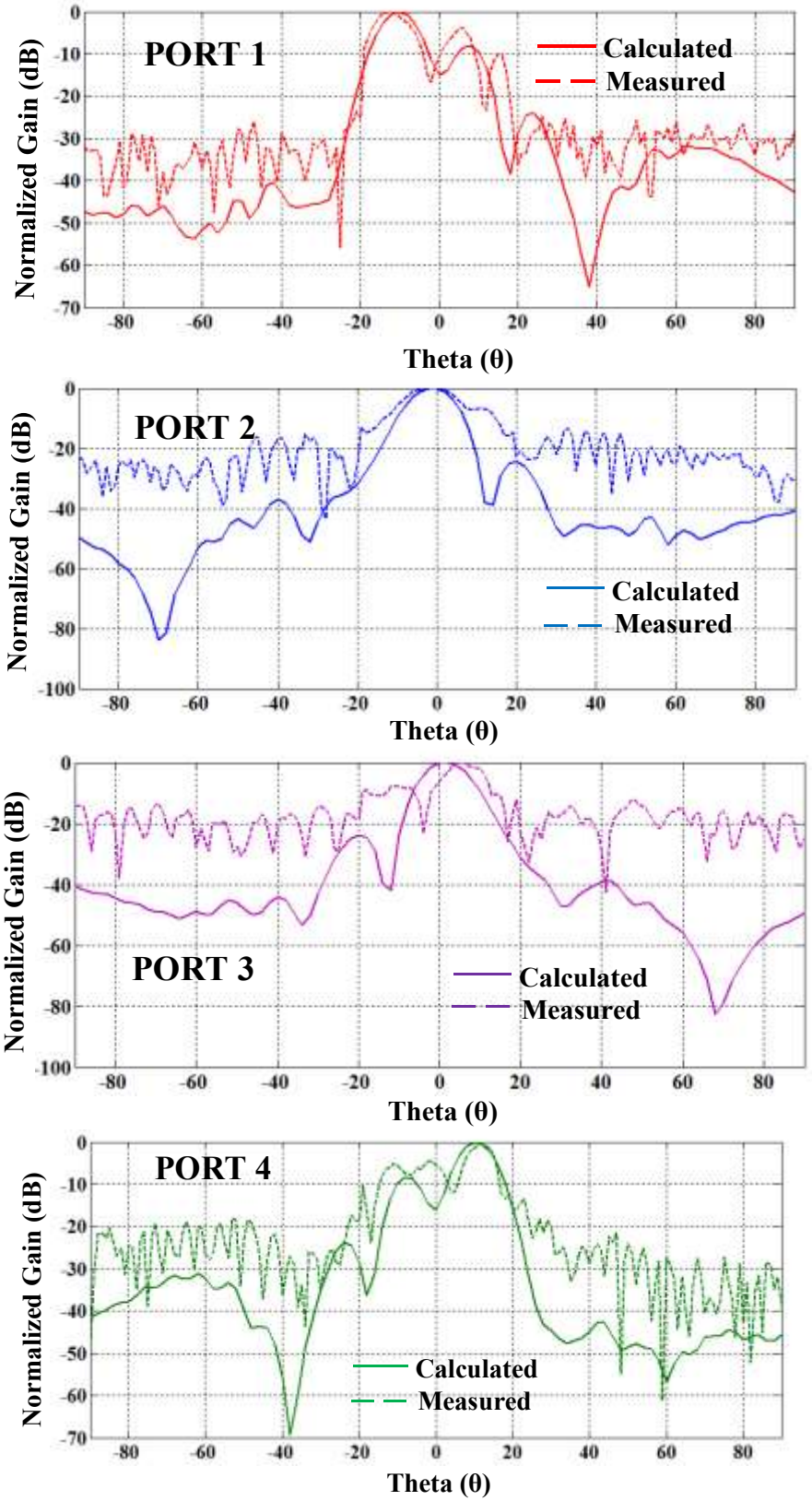

Fig. 5.18 Normalized Gain of 4 × 4 AFLTSA subarray when excited from port 1-4.

Table 5.2: Calculated and measured performance characteristics of 4 × 4 AFLTSA subarray.

F(GHz)	Total Gain (dB)			Total Gain (dB)		
	Calculated	Measured (P1/P4)		Calculated	Measured (P2/P3)	
31	11.2	10.1	10.23	12.5	11.42	11.67
32	11.7	10.35	10.42	11.36	10.2	10.25
32.5	12.63	11.45	11.6	14.94	13.8	13.86
33	11.3	10.23	10.5	13.6	12.45	12.61
34	12.07	10.94	11.1	14.24	13.15	13.23
35	11.3	10.05	10.3	13.92	12.74	12.82
36	10.8	9.7	9.8	12.34	11.32	11.45

5.6 Summary

In this chapter, a beamforming subarray for two and four AFLTSA elements is presented. The design methodology for analyzing the symmetrical beamforming network is presented including parametric analysis for both subarrays. The fabrication and measurement setup requirements are discussed along with the calculated and measured results for 2 × 2 and 4 × 4 AFLTSA subarrays. It is found that there is a good agreement between the simulated and measured results thus making this proposed structure as a good candidate for performing beamforming at millimeter wave band.

Chapter 6: Conclusions

6.1 Conclusions

The work presented in this thesis aims towards design of millimeter wave antennas with their potential applications use in wireless communications, imaging and detection of hidden objects. Due to high atmospheric abortion at millimeter wave frequencies, high gain antennas are required. In this thesis, a high gain endfire antenna is analyzed in different configurations such as array system and beamforming networks. Besides high gain antenna, the antenna configurations possess low loss and cost with narrow beamwidth making it suitable for millimeter wave applications.

In chapter 3, antipodal fermi linear tapered slot antenna (AFLTSA), substrate integrated circuits and beamforming networks are studied. The single element antenna having sine corrugations on the edges to improve the radiation characteristics of the antenna is designed. It possess wide impedance bandwidth of more than 30 % with a high gain of 12.6 dB and wide beamwidth of 30° and 40.57° in E-plane and H-plane, respectively. It also possess low side lobe level of -17.85 dB in both planes. The substrate integrated waveguide technology is used in this antennas' configuration in an array system and beamforming networks due to low loss, high quality factor and easy integration of whole system on a single substrate at MMW frequencies.

In chapter 4, 1 × 8 AFLTSA array is presented using compact SIW power divider. The matching characteristics of this unequal power divider is studied and simulated results are presented. This array configuration has a wide bandwidth of 14.7 % (30-35 GHz) along with high gain of 20.4 dB. The E-plane and H-plane side lobe levels are improved and are

better than -25 dB and -15 dB, respectively. This radiated beam achieves a narrow 3 dB beamwidth of 8.3° in the E-plane, which makes it a suitable candidate for detecting hidden objects in a particular desired direction. The efficiency of this array structure is greater than 90% over the impedance bandwidth.

In chapter 5, two and four element AFLTSA subarrays are presented to perform beamforming operation, which also has the same criteria of obtaining high gain and narrow beamwidth characteristics. Two beamforming networks using multimode section technique are simulated, analyzed and presented in this chapter. The subarrays are designed with the help of these beamforming networks and are fabricated. The measured results show a good agreement with the simulated results. A 2 × 2 subarray structure achieves a wide impedance bandwidth between 29-36 GHz along with beam rotation at ±6° when excited from either port. The beam possess a high gain of 12.2 dB with a narrow beamwidth of 19.93° at 32.5 GHz. This configuration has the capacity to achieve gain between 10.5-12.2 dB with radiation efficiency better than 89% over the impedance bandwidth. Furthermore, a 4 × 4 subarray structure is designed to increase the gain and make the radiated beam narrower. Although, it is more complex to design this configuration with more number of input ports and elements but the results obtained are much better than two element subarray. The return loss is better than -10 dB from 31-36 GHz and it possess a measured gain of 11.45/11.6 dB (±10°) -13.8/13.86 dB (±2°) dB when excited from port 1/4 and 2/3, respectively at 32.5 GHz. Moreover, the calculated 3 dB beamwidth is 11.85° and 13.05° which makes it suitable for millimeter wave applications.

6.2 Contributions

The main contribution of this thesis is towards the design of millimeter wave antennas and can be divided into the following specialized areas:

a) The study of substrate integrated power divider and beamforming networks which makes this technology suitable for MMW satellite and mobile communications. This thesis introduces the performance parameters analysis of single endfire antenna in array and beamforming network form using same substrate material and design specifications.

b) The design of 1 × 8 AFLTSA array is a suitable candidate for future 5G network communications with high gain of 20.4 dB and narrow beamwidth of 8.3° at 32.5 GHz. There are low SIW array feeding losses in comparison to microstrip array deigns at millimeter wave frequencies and this proposed structure is able to achieve SLL better than 25 dB in E-plane and 15 dB in H-plane.

c) The 2 × 2 and 4 × 4 subarray beamforming networks are designed for millimeter wave wireless communications and detection and target tracking of hidden objects applications. Such applications need high gain antennas with narrow beamwidth along with beam scanning of the antenna. This work illustrates multibeam antenna with compact structure and high efficiency.

6.3 Future Works

This thesis deals with array configuration and beamforming networks of endfire antennas. Firstly, this work is a start to understand the beamforming networks using modern improvised techniques and further can be implemented for beamforming operations using

switches and passive components. This work is recent at MMW and can be extensively analyzed with digital techniques as well. Secondly, as we know the gain increases with increase in frequency, therefore these array and beamforming configurations can be simulated, optimized and fabricated for 60 GHz also.

In terms of improving of current designs, the high gain antennas with shorter antenna length should be designed in order to make more compact structures at high frequencies.

References

[1] T. S. Rappaport, R. Mayzus, Y. Azar, K. Wang, G. N. Wong, J. K. Schulz, M. Samimi and F. Gutierrez, "Millimeter Wave Mobile Communications for 5G Cellular: It Will Work!," in *IEEE Access, vol. 1, pp. 335–349, 2013.*.

[2] A. Ghosh, T. A. Thomas, M. C. Cudak, R. Ratasuk, P. Moorut, F. W. Vook, T. S. Rappaport, G. R. MacCartney, S. Sun and S. Nie, "Millimeter-Wave Enhanced Local Area Systems: A High-Data-Rate Approach for Future Wireless Networks," in *IEEE Journal on Selected Areas in Communications, vol. 32, no. 6, pp. 1152–1163, June 2014*.

[3] Y. Niu, Y. Li, D. Jin, L. Su and A. V. Vasilakos, "A Survey of Millimeter Wave (mmWave) Communications for 5G: Opportunities and Challenge," in *Computer Science - Networking and Internet Architecture, 2015.* .

[4] T. S. Rappaport, S. Sun, R. Mayzus, H. Zhao, Y. Azar, K. Wang, G. N. Wong, J. K. Schulz, M. Samimi and F. Gutierrez, "Millimeter Wave Mobile Communications for 5G Cellular: It Will Work!," in *IEEE Access, vol. 1, no. , pp. 335-349, 2013.*.

[5] F. Gutierrez, S. Agarwal, K. Parrish and T. S. Rappaport, "On- chip integrated antenna structures in CMOS for 60 GHz WPAN systems," in *IEEE J. Sel. Areas Commun., vol. 27, no. 8, pp. 1367–1378, Oct. 2009.* .

[6] F. Rusek, D. Persson, B. Lau, E. Larsson, T. Marzetta, O. Edfors and F. Tufvesson, "Scaling up MIMO: Opportunities and challenges with very large arrays," in *IEEE Signal Process. Mag., vol. 30, no. 1, pp. 40–60, Jan. 2013.* .

[7] E. TC48 and E. s. 387, "High rate 60 GHz PHY, MAC and HDMI PAL," Dec. 2008..

[8] "IEEE 802.15 WPAN Millimeter Wave Alternative PHY Task Group 3c (TG3c)," Available: http://www.ieee802.org/15/pub/TG3c.html...

[9] "Draft Standard for Information Technology–Telecommunications and Information Exchange Between Systems–Local and Metropolitan Area Networks–Specific

Requirements–Part 11: Wireless LAN Medium Access4: Enhancements for Very High Throughput in the 60 Ghz Band," IEEE P802.11ad/D9.0, Oct. 2012..

[10] T. Rappaport, E. Ben-Dor, J. Murdock and Y. Qiao, "38 GHz and 60 GHz angle-dependent propagation for cellular & peer-to-peer wireless communications," in Communications (ICC)," in *2012 IEEE International Conference on , vol., no., pp.4568,4573, 10-15 June 2012*.

[11] H. Zhao, R. Mayzus, S. Sun, M. Samimi, J. Schulz, Y. Azar, K. Wang, G. Wong, F. Gutierrez and T. Rappaport, "28 GHz Millimeter Wave Cellular Communication Measurements for Reflection and Penetration Loss in and around Buildings in New York City," in *Communications (ICC), 2013 IEEE International Conference on , vol., no., pp.5163,5167, 9-13 June 2013*.

[12] T. Rappaport, J. Murdock and F. Gutierrez, "State of the Art in 60-GHz Integrated Circuits and Systems for Wireless Communications," in *Proceedings of the IEEE , vol.99, no.8, pp.1390,1436, Aug. 2011*.

[13] K. Huang and D. Edwards, Millimetre Wave Antennas for Gigabit wireless communication, John Wiley and Sons Inc., 2008.

[14] A. Elboushi, O. Haaraz and A. Sebak, "High gain circularly polarized slot-coupled antenna for millimeter wave applications," in *Microwave and Optical Technology Letters/Vol.56,No.11, November 2014*.

[15] P. Bhartia and I. J. Bahl, Millimeter Wave Engineering and Applications, John Wiley & sons Inc., 1984.

[16] H. Singh, J. Oh, C. Kweon, X. Qin, H. Shao and C. Ngo, "A 60 GHz wireless network for enabling uncompressed video communication," in *IEEE Communications Magazine, vol. 46, no. 12, pp. 71–78, December 2008*.

[17] R. Taori and A. Sridharan, "Point-to-multipoint in-band mmwave backhaul for 5G networks," in *IEEE Communications Magazine, vol. 53, no. 1, pp. 195–201, January 2015*.

[18] R. Munson, "Conformal microstrip antennas and microstrip phased arrays," in *IEEE Transactions on Antennas and Propagation, vol. 22, no. 1, pp. 74-78, Jan 1974*.

[19] H. Elsadek, Microstrip Antennas for Mobile Wireless Communication Systems, Mobile and Wireless Communications Network Layer and Circuit Level Design, 2010.

[20] R. A. Alhalabi and G. M. Rebeiz, "High-Gain Yagi-Uda Antennas for Millimeter-Wave Switched-Beam Systems," in *IEEE Transactions on Antennas and Propagation, vol. 57, no. 11, pp. 3672-3676, Nov. 2009*.

[21] A. Elboushi and A. Sebak, "High-Gain Hybrid Microstrip/Conical Horn Antenna for MMW Applications," in *IEEE Antennas and Wireless Propagation Letters, vol. 11, no. , pp. 129-132, 2012*.

[22] R. K. Mongia, A. Ittipiboon and M. Cuhaci, "Measurement of radiation efficiency of dielectric resonator antennas," in *IEEE Microwave and Guided Wave Letters, vol. 4, no. 3, pp. 80-82, March 1994*.

[23] Q. Lai, G. Almpanis, C. Fumeaux, H. Benedickter and R. Vahldieck, "Comparison of the Radiation Efficiency for the Dielectric Resonator Antenna and the Microstrip Antenna at Ka Band," in *IEEE Transactions on Antennas and Propagation, vol. 56, no. 11, pp. 3589-3592, Nov. 2008*.

[24] W. M. A. Wahab, D. Busuioc and S. Safavi-Naeini, "Low Cost Planar Waveguide Technology-Based Dielectric Resonator Antenna (DRA) for Millimeter-Wave Applications: Analysis, Design, and Fabrication," in *IEEE Transactions on Antennas and Propagation, vol. 58, no. 8, pp. 2499-2507, Aug. 2010*.

[25] K. Wu, D. Deslandes and Y. Cassivi, "The substrate integrated circuits - a new concept for high-frequency electronics and optoelectronics," in *Telecommunications in Modern Satellite, Cable and Broadcasting Service, 2003. TELSIKS 2003. 6th International Conference on, 2003, pp. P-III-P-X vol.1*.

[26] D. Deslandes and K. Wu., "Integrated microstrip and rectangular waveguide in planar form," in *IEEE Microwave and Wireless Components Letters, vol. 11, no. 2, pp. 68-70, Feb. 2001.*.

[27] D. Deslandes and K. Wu, "Integrated transition of coplanar to rectangular waveguides," in *IEEE International Microwave Symposium, May 2001, pp. 619–622*.

[28] D. Deslandes and K. Wu, "Analysis and design of current probe transition from grounded coplanar to substrate integrated rectangular waveguide," in *IEEE Transactions on Microwave Theory and Techniques, 53(8): 2487–2494, 2005*.

[29] Elboushi, H. O. A. and A. Sebak, "High gain circularly polarized slot-coupled antenna for millimeter wave applications," in *Microw. Opt. Technol. Lett., 56: 2522–2526. doi: 10.1002/mop.28637*, 2014.

[30] K. S. Yngvesson, T. L. Korzeniowski, Y. S. Kim, E. L. Kollberg and J. F. Johansson, "The tapered slot antenna-a new integrated element for millimeter-wave applications," in *IEEE Transactions on Microwave Theory and Techniques, vol. 37, no. 2, pp. 365-374, Feb 1989*.

[31] D. Schaubert, E. Kollberg, T. Korzeniowski, T. Thungren, J. Johansson and K. Yngvesson, "Endfire tapered slot antennas on dielectric substrates," in *IEEE Transactions on Antennas and Propagation, vol. 33, no. 12, pp. 1392-1400, Dec 1985*.

[32] Z. Briqech, J. Robitaille, K. Bishyk, K. Abdo, D. Bhogal and A. Sebak, "High gain antipodal tapered slot antenna With sine-shaped corrugation and fermi profile substrate slotted cut-out for MMW 5G," in *Millimeter Waves (GSMM), 2015 Global Symposium On, Montreal, QC, 2015, pp. 1-3*.

[33] S. Sugawara, Y. Maita, K. Adachi, K. Mori and K. Mizuno, "A mmwave tapered slot antenna with improved radiation pattern," in *Microwave Symposium Digest, Denver, CO, 1997, pp. 959–962.*.

[34] N. Ghassemi and K. Wu, "Planar High-Gain Dielectric-Loaded Antipodal Linearly Tapered Slot Antenna for E- and W-Band Gigabyte Point-to-Point Wireless Services," in *IEEE Transactions on Antennas and Propagation, vol. 61, no. 4, pp. 1747-1755, April 2013*.

[35] I. Mohamed, Z. Briqech and A. R. Sebak, "High-gain dielectric-loaded antipodal Fermi tapered slot antenna for MM-wave applications," in *Antenna Technology*

and Applied Electromagnetics (ANTEM), 2014 16th International Symposium on, Victoria, BC, 2014, pp. 1-2.

[36] B. Biglarbegian, M. Fakharzadeh, D. Busuioc, M. R. Nezhad-Ahmadi and S. Safavi-Naeini, "Optimized Microstrip Antenna Arrays for Emerging Millimeter-Wave Wireless Applications," in *IEEE Transactions on Antennas and Propagation, vol. 59, no. 5, pp. 1742-1747, May 2011*.

[37] J. F. Zurcher, "The SSFIP: a global concept for high-performance broadband planar antennas," in *Electronics Letters, vol. 24, no. 23, pp. 1433-1435, 10 Nov. 1988*.

[38] R. A. Alhalabi and G. M. Rebei, "High-Efficiency Angled-Dipole Antennas for Millimeter-Wave Phased Array Applications," in *IEEE Transactions on Antennas and Propagation, vol. 56, no. 10, pp. 3136-3142, Oct. 2008*.

[39] W. M. Abdel-Wahab, Y. Wang and S. Safavi-Naeini, "Ka-band SIW-integrated DRA linear array based on longitudinal slot coupling," in *Antennas and Propagation Society International Symposium (APSURSI), 2013 IEEE, Orlando, FL, 2013, pp. 1876-1877*.

[40] W. M. Abdel-Wahab, D. Busuioc and S. Safavi-Naeini, "Millimeter-Wave High Radiation Efficiency Planar Waveguide Series-Fed Dielectric Resonator Antenna (DRA) Array: Analysis, Design, and Measurements," in *IEEE Transactions on Antennas and Propagation, vol. 59, no. 8, pp. 2834-2843, Aug. 2011*.

[41] Y. M. Cheng, P. Chen, W. Hong, T. Djerafi and K. Wu, "Substrate-Integrated-Waveguide Beamforming Networks and Multibeam Antenna Arrays for Low-Cost Satellite and Mobile Systems," in *IEEE Antennas and Propagation Magazine, vol. 53, no. 6, pp. 18-30, Dec. 2011*.

[42] M. Donelli, L. F. R. Azaro and A. Massa, "A Planar Electronically Reconfigurable Wi-Fi Band Antenna Based on a Parasitic Microstrip Structure," in *IEEE Antennas and Wireless Propagation Letters, vol. 6, no. , pp. 623-626, 2007*.

[43] H. R, Phased array antennas, New York: John WIley, 2009.

[44] Y. J. Cheng, W. Hong, K. Wu, Z. Q. Kuai, C. Yu, J. X. Chen, J. Zhou and H. J. Tang, "Substrate Integrated Waveguide (SIW) Rotman Lens and Its Ka-Band Multibeam Array Antenna Applications," *Antennas and Propagation, IEEE Transactions on , vol.56, no.8, pp.2504-2513, Aug. 2008.*

[45] Y. J. Cheng, W. Hong, K. Wu and Y. Fan, "Millimeter-Wave Substrate Integrated Waveguide Long Slot Leaky-Wave Antennas and Two-Dimensional Multibeam Applications," in *IEEE Transactions on Antennas and Propagation, vol. 59, no. 1, pp. 40-47, Jan. 2011*.

[46] Y. J. Cheng, W. Hong and K. Wu, "Millimeter-Wave Half Mode Substrate Integrated Waveguide Frequency Scanning Antenna With Quadri-Polarization," in *IEEE Transactions on Antennas and Propagation, vol. 58, no. 6, pp. 1848-1855, June 2010*.

[47] Y. J. Cheng, W. Hong and K. Wu, "Millimeter-Wave Substrate Integrated Waveguide Multibeam Antenna Based on the Parabolic Reflector Principle," *Antennas and Propagation, IEEE Transactions on , vol.56, no.9, pp.3055-3058, Sept. 2008.*

[48] Constantine A. Balanis, Advanced Engineering Electromagnetics, 2nd.: John Wiley & Sons.

[49] D. Davidson, An overview of Computational Electromagnetics for RF and Microwave applications, Computational Electromagnetics for RF and Microwave Engineering Second., Cambridge University Press, 2011.

[50] D. B. Davidson, Computational Electromagnetics for RF and Microwave Engineering, Second Edition, Cambridge University Press, 2010.

[51] A. H. f. A. Simulation. [Online]. Available: http://www. ansys. com/Products/Simulation+Technology/ElectronicsRF+&+Microwave.

[52] M. Clements and T. Weiland, "Discrete electromagnetism with the Finite Integration Technique," in *Progress In Electromagnetics Research, vol. 32, pp. 65–87, 2001.*.

[53] K. Wu, "Substrate Integrated Circuits (SICs) for Low-Cost High-Density Integration of Millimeter-Wave Wireless Systems," *Proc RWS2008, Jan. 2008, pp.683-686.*

[54] D. D and L. A. P. B. K. W. Perregrini, "Dispersion characteristics of substrate integrated rectangular waveguide," in *IEEE Microwave Wireless Compon. Lett., vol. 12, pp. 333-335, Sept. 2002*.

[55] J. Rayas-Sanchez and V. Gutierrez-Ayala, "A general EM-based design procedure for single-layer substrate integrated waveguide interconnects with microstrip transitions," *Microwave Symposium Digest, 2008 IEEE MTT-S International , vol., no., pp.983-986, 15-20 June 2008.*

[56] D.-C. Chang, B.-H. Zeng and J.-C. Liu, "“Modified antipodal Fermi antenna with piecewise-linear approximation and shaped-comb corrugation for ranging applications," in *Microw., Antennas Propag., vol. 4,no. 3, pp. 399–407, Mar. 2010.*.

[57] Z. Ma and E. Yamashita, "Efficient fullwave analysis of a waveguide T-junction with an inductive post.," in *1994 Asia-Pacific Microwave Conference Proceedings, December 1994, pp. 259–262*.

[58] X. Xu, R. G. Bosisio and K. Wu, "A new six-port junction based on substrate integrated waveguide technology," in *IEEE Transactions on Microwave Theory and Techniques, 53(7): 2267–2273, 2005*.

[59] Y. J. Cheng, Substrate Integrated Antennas and Arrays, CRC Press, 2014.

[60] Y. Cheng, W. Hong and K. Wu, "Design of a mult imode beamforming network based on the scattering matrix analysis," in *Sci China SerF-Inf Sci, 2009, 52(7): 1258–1265*.

[61] Y. J. Cheng and Y. Fan, "Millimeter-Wave Miniaturized Substrate Integrated Multibeam Antenna," *Antennas and Propagation, IEEE Transactions on , vol.59, no.12, pp.4840-4844, Dec. 2011.*

[62] Y. Cheng, W. Hong and K. Wu, "Design of a multimode beamforming network based on the scattering matrix analysis," *Sci China SerF-Inf Sci, 2009, 52(7): 1258–1265,.*

[63] J. Puskely and T. Mikulasek, "Compact wideband Vivaldi antenna array for microwave imaging applications," *Antennas and Propagation (EuCAP), 2013 7th European Conference on , vol., no., pp.1519-1522, 8-12 April 2013.*

[64] s. microwave, "2.92 mm"K" connector series," [Online]. Available: http://mpd.southwestmicrowave.com/showImage.php?image=823&name=2.92_Connectors.pdf.

[65] S. Microwave, "Optimizing Test Boards for 50 GHz End Launch Connectors," [Online]. Available: http://mpd.southwestmicrowave.com/showImage.php?image=439.

[66] L. Frenzel, Communication Electronics: Principles and Applications, McGraw-Hill Companies, 2001.

[67] Y. J. C. e. al., "Substrate Integrated Waveguide (SIW) Rotman Lens and Its Ka-Band Multibeam Array Antenna Applications," in *EEE Transactions on Antennas and Propagation, vol. 56, no. 8, pp. 2504-2513, Aug. 2008*.

List of publications

[C1] **Sh.Gupta**, M. Akbari, R. Movahedinia, S. Zarbakhsh, and A. R. Sebak, "Low-Side Lobe Level Aperture Coupled Dielectric Resonator Antenna Array Fed by SIW" Accepted in EuCAP 2016

[C2] **Shraman Gupta**, M.Akbari, Abdelrazik Sebak, “SIW Beamforming of 2 × 2 and 4 × 4 AFLTSA Arrays for MMW Applications" Accepted in Antennas and Propagation Society International Symposium (APS/URSI), 2016

[C3] **Shraman Gupta**, M.Akbari, Abdelrazik Sebak, “High Gain Antipodal Fermi-Linear Tapered Slot Antenna (AFLTSA) Array fed by SIW for MMW

Applications" Accepted in Antenna Technology and Applied Electromagnetics (ANTEM) 2016

[C4] **Shraman Gupta**, M.Akbari, Abdelrazik Sebak, " Comparison of Narrow/Wide Beamwidth AFLTSA and Yagi Antenna for MMW Applications " Accepted in PIERS 2016 (Progress In Electromagnetics Research Symposium)

[Co1] M. Akbari , **Sh.Gupta**, R. Movahedinia, S. Zarbakhsh, and A. R. Sebak, "Bandwidth Enhancement of 4×4 Subarrays Circularly Polarized Rectangular Dielectric Resonator Antenna by Sequential Feeding Network" Accepted in EuCAP 2016

[Co2] M.Akbari, **Sh. Gupta**, Abdelrazik Sebak, "Sequential Feeding Networks for Subarrays of Circularly Polarized patch Antenna " Accepted in Antennas and Propagation Society International Symposium (APS/URSI), 2016

[Co3] M.Akbari, **Sh. Gupta,** A. R. Sebak, "High Gain Circularly-Polarized Fabry-Perot Dielectric Resonator Antenna for MMW applications " Accepted in Antennas and Propagation Society InternationaL SYMPOSIUM (APS/URSI), 2016

[Co4] M. Akbari, **Sh. Gupta**, S. Zarbakhsh and A. R. Sebak, "A Linear to Circular polarizer based on Frequency Selective Surface Operating 30GHz Applications " Accepted in Antenna Technology and Applied Electromagnetics (ANTEM) 2016.

[Co5] Mohammad Akbari Choubar, **Shraman Gupta**, Reza Movahedinia, and Abdel Razik Sebak, "Comparison of Sequential Subarrays of Circularly Polarized DR and Patch Antennas Based on Hybrid Ring Feeding in MMW" Accepted in PIERS 2016 (Progress In Electromagnetics Research Symposium)